

# An $O(n)$ Time Discrete Relaxation Architecture for Real-Time Processing of the Consistent Labeling Problem

UUCS-TR-86-116

*Jun Gu, Wei Wang\* and Thomas C. Henderson*

*Department of Computer Science  
\* Department of Electrical Engineering*

*University of Utah  
Salt Lake City, UT 84112*

*December 1986*

## Abstract

Discrete relaxation techniques have proven useful in solving a wide range of problems in digital signal and digital image processing, artificial intelligence, operations research, and machine vision. Much work has been devoted to finding efficient hardware architectures. This paper shows that a conventional hardware design for a Discrete Relaxation Algorithm (DRA) suffers from  $O(n^2m^3)$  time complexity and  $O(n^2m^2)$  space complexity. By reformulating DRA into a parallel computational tree and using a multiple tree-root pipelining scheme, time complexity is reduced to  $O(nm)$ , while the space complexity is reduced by a factor of 2. For certain relaxation processing, the space complexity can even be decreased to  $O(nm)$ . Furthermore, a technique for dynamic configuring an architectural wavefront is used which leads to an  $O(n)$  time highly configurable DRA3 architecture.

## Index Terms

Algorithm-configured dynamic architectural wavefront system, associative circular pipelining, data-structured computer architecture, Consistent labeling problem (CLP), data-communication-intensive VLSI computation, Discrete Relaxation Algorithm (DRA), interleaved processing, multiprocessor architecture, recursive systolic computation, VLSI.

---

• This work is supported in part by National Science Foundation Grants MCS-82-21750, DCR-85-06393, and DMC-85-02115; and

in part by a University of Utah Research Fellowship and an ACM/IEEE Scholarship.

● The UUCS-TR-86-008 contains a DRA2 architecture which is good for DRA computation only with  $n = m = 8$ . Upon inquiry of its extensibility for computing of the large size DRA problems, this paper, in addition to presents a faster DRA3 architecture, it also generalizes DRA2 for arbitrary size of DRA problems (as long as chip size permits) with the descriptions that differentiates the object number  $n$  and label number  $m$ , throughout the paper.

● A short version of this manuscript is on IEEE Trans. on Pattern Analysis and Machine Intelligence, Vol. PAMI-9, pp. 816-831. Nov. 1987.

## Table of Contents

### 1. Introduction and Motivation

1.1 Consistent Labeling Problem and Discrete Relaxation Operator

1.2 Related Work

### 2. Discrete Relaxation Algorithm

2.1 Boolean Formulation of Discrete Relaxation Algorithm

2.2 An Example of Region Coloring Problem

### 3. The Hardware Implementation Problems for DRA

3.1 Assumptions and Statements

3.2 DRA Hardware Implementation

### 4. A Conventional DRA1 Design and the Complexity Analysis

### 5. Parallel Tree-Root Pipelining and the DRA2 System

5.1 A Parallel Tree-Structured Reformulation for DRA

1. Constructing the Parallel Computation Tree

2. Speeding Up Iteration

3. Introducing a Time Dimension in the Computation

5.2 Implementation Issues for the DRA2 Chip

1. System Architecture and Block Diagram

2. Multiprocessor SIMD Array and the Cell Design

3. Circuit Features and Design Techniques

5.3 Performance Evaluation

5.4 The PPL Layout for DRA2 System

### 6. An $O(n)$ Time Algorithm-Configured Dynamic Architectural Wavefront System

6.1 Complexity Issues Revisited

6.2  $C_{ij}(k,p)$ -Pattern Distribution Analysis

6.3 A Dynamically Configurable DRA3 Architecture

1. The Architectural-Computational Wavefront (ACW) Notation

2. Dynamic Configuring the DRA3 Architectural Wavefront

**7. Conclusions**

**References**

## List of Figures

- Figure 1:** Leaf Node for Computing  $l_{jp} \times \Lambda_{ij}(k,p)$
- Figure 2:** Modified Leaf Node Computation for  $l_{jp} \times \Lambda_{ij}(k,p)$
- Figure 3:** A Parallel Tree for Computing  $n^{\text{th}} l_{ik}$
- Figure 4:** Circuit Block Diagram for the DRA2 System
- Figure 5:** Basic Principle of the Parallel DRA2 System
- Figure 6:** Two Cells in Multiprocessor DRA2 Array
- Figure 7:** Construction of SIMD Multiprocessor Array Using Cell-A and Cell-B
- Figure 8:** Computational Wavefront Pipelining and Circulation for Interleaved Processing
- Figure 9:** Broadcasting Scheme for  $b_k$  Signal
- Figure 10:** Associative Circular Pipelining
- Figure 11:** Self-Timed Synchronization
- Figure 12:** State Graph of Finite State Machine
- Figure 13:** The PPL Layout of the Multiprocessor SIMD DRA2 System
- Figure 14:** The Photomicrograph of the DRA2 Chip
- Figure 15:** The  $C_{1j}(k,p)$  Pattern for generating  $l_{1k}$ 's
- Figure 16:** The  $C_{2j}(k,p)$  Pattern for generating  $l_{2k}$ 's
- Figure 17:** A Circularly Skewed  $C_{ij}(k,p)$ -Pattern when Generating  $l_{ik}$ 's
- Figure 18:** A Candidate Design for DRA3 System
- Figure 19:** The DRA3 Architecture
- Figure 20:** A  $C_{ij}(k,p)$ -Pattern under Dynamic Reconfiguration of DRA3

## 1. Introduction and Motivation

### *1.1 Consistent Labeling Problem and Discrete Relaxation Operator*

The **Consistent Labeling Problem (CLP)** [4,5,6] has long been viewed as a computational model based on a unit constraint relation containing  $2N$ -tuples of units and labels which specifies which  $N$ -tuples of units are compatible with which  $N$ -tuples of labels.

A variety of problems in digital signal and digital image processing, artificial intelligence, operations research, symbolic logic, computer graphics, robot vision, and robot manipulation are special cases of CLP. Some problems that are naturally viewed in this way are finding  $N$ -ary relations such as transitive closure [24], detection of the graph and subgraph isomorphism [3,18], data-base consistency-maintenance, query-answering and redundancy-checking [30], the relational homomorphism problem [4], the constraint satisfaction problem [23,25], the automata homomorphism problem [17], finding spanning trees and Euler tours in a graph [32], the graph coloring problem [18], the packing problem [22], scene and edge labeling problems [4], the scene and shape matching problem [24], many puzzles such as the latin square puzzle [4,28], the cryptarithmic puzzle [31], determining satisfiability of propositional logic statements and theorem proving [26], space planning problem [29], and finding Hamiltonians in a graph [24].

One general technique for finding a consistent labeling is depth-first search but it suffers from thrashing [4]. The search procedure fixes labels to units as long as it can find a label for each new unit that is compatible, according to the constraint relation, with the labels already fixed to previous units. Whenever the procedure cannot find a label for a new unit, it backtracks to the previous unit and tries to find a different label for that unit. If the procedure finds a label for all units, it has found a consistent labeling. If the procedure backs up all the way to the first unit without finding any consistent labelings and there are no more possible labels for the first unit, the procedure fails and there exists no consistent labeling. Montanari [33] pointed out that this problem is NP-complete.

The *arc-consistency algorithms* filter the problem variable domain to eliminate unacceptable candidate values, while *path-consistency algorithms* filter problem constraints to eliminate unacceptable tuples. For example, the Waltz filtering algorithm reduces any binary compatibility relation to its maximal arc consistent subset [35]. Ullman [3] applies the Waltz algorithm to the subgraph isomorphism problem. Montanari [33] discusses various aspects of the constrained labeling problem for binary relations. The **Discrete Relaxation Algorithm (DRA)**, described in [9,21],

is a look-ahead operator which takes polynomial time in accelerating tree search required to find the consistent labelings. Henderson [9] also noted that DRA is a restriction of the classical relaxation techniques to systems of Boolean inequalities which take values over the two element set  $\{0,1\}$ .

## ***1.2 Related Works***

Since the introduction of the discrete relaxation technique in the mid-seventies, many DRA applications have been found, and much work has been done to develop optimal DRA algorithms [8,9,21]. On the other hand, people have also tried to build efficient hardware architectures to support real-time DRA processing. Unfortunately, due to high computational cost including space complexity, time complexity, and data communication cost, a conventional hardware architecture implementation is not feasible [13]. Current research in this aspect is blocked, and has appeared only in a virtual software simulator format [7].

The research described in this paper concerns the hardware implementation of discrete relaxation architecture. In section 2 we briefly describe the Discrete Relaxation Algorithm, and give an example for solving the region coloring problem. Then we define the DRA hardware implementation problem in section 3. Complexity analyses and our first design of the DRA1 chip are presented in section 4. In section 5, we concentrate on the design of the parallel DRA computational tree and a tree-root pipelining scheme, and its corresponding  $O(nm)$  time SIMD multiprocessor architecture DRA2. Finally, it is shown that we have adopted a dynamically configurable, highly parallel routing scheme on the DRA3 switch lattice, so that an  $O(n)$  time algorithm-configured architectural wavefront system, DRA3, is found.

These three architectures are designed for the same 8-object 8-label DRA problems. The first two systems are implemented using PPL (Path Programmable Logic) [36] at the University of Utah. The DRA1 chip requires two 4K memory blocks and maximum execution time of over an hour in a  $3\ \mu$  NMOS process, which makes such a hardware implementation infeasible [11, 13]. The DRA2 design eliminates excessive memory requirements and performs the DRA computation in microseconds, at the worst case in milliseconds. This chip was fabricated using a  $3\ \mu$  NMOS process by MOSIS [11,15]. DRA3 will be fabricated using an  $1.0\ \mu$  GaAs technology. The clock speed of DRA3 is expected to be over, at least, 500 MHz [12]. In this paper, we try to describe our research ideas and the architectural concepts for these DRA architectures as concisely as possible. For detailed reference see [11-15].

## 2. The Discrete Relaxation Algorithm (DRA)

### 2.1 Boolean Formulation of Discrete Relaxation Algorithm

Instead of seeking a real number solution in a numerical relaxation situation [19], the solution to be found in the discrete relaxation case involves the assignment of a set of *labels* at each unknown such that some constraint relation among the labels is satisfied by neighboring unknowns [8,9]. Whereas the unknowns in numerical relaxation take on real number values, the unknowns in a *labeling problem* take on a Boolean vector value with each element in the vector corresponding to a possible label.

The generalized problem involves a set of unknowns which usually represents a set of objects to be given names, a set of labels which are the possible names for the unknown, and a *compatibility model* containing ordered groups of units which mutually constrain one another and ordered groups of unit-label pairs which are compatible. The compatibility model is sometimes called a *world model*. This model tells us which objects mutually constrain one another and which labelings are permitted or legal for those objects which do constrain one another. The problem is to find a label for each object such that the resulting set of object-label pairs is consistent with the constraints of the world model.

Boolean vector operations are denoted by  $'$ ,  $\times$ ,  $t$ ,  $*$ ,  $+$  and  $\cdot$  which represent complementation, vector multiplication, transpose, Boolean "and," Boolean "or," and Boolean vector dot product, respectively. Our basic definitions which are used in formulating DRA are given in:

Definition 1: Let  $U = \{u_1, \dots, u_n\}$  be the set of unknowns, and  $\Lambda = \{\lambda_1, \dots, \lambda_m\}$  be the set of possible labels. Then

1.  $C$  is an  $m$  by  $m$  *compatibility matrix for label pairs*, where  $C(i,j)=1$  if  $\lambda_i$  is compatible with  $\lambda_j$ ; 0 otherwise.
2.  $\Lambda_i = (l_1, \dots, l_m)^t$  is the column vector describing the set of labels (i.e., zero or one) possible for  $u_i$ , where  $l_j=1$  if  $\lambda_j$  is compatible with  $u_i$ ; 0 otherwise.
3.  $\Lambda_{ij} = (\Lambda_i \times \Lambda_j^t) * ((\text{Nei}(i,j)'E) + C)$  is an  $m$  by  $m$  *compatibility matrix for  $u_i$  and  $u_j$* , where  $E$  is the  $m$  by  $m$  matrix for all 1's, and  $\text{Nei}(i,j) = 1$  if  $u_i$  neighbors  $u_j$ ; 0 otherwise. We use  $\Lambda_k$  denotes  $k^{\text{th}}$  row of  $\Lambda_{ij}$ .

Definition 2: A *labeling* is a vector  $L = (L_1, \dots, L_n)^t$ , where  $L_i = (l_1, \dots, l_m)$  in  $\Lambda_i$  is a Boolean vector with  $l_{ij} = 1$  if

label  $\lambda_j$  is a possible label for object  $u_i$ ; 0 otherwise.

Definition 3: A labeling is *consistent* if for every  $i$  and  $k$ ,

$$l_{ik} \leq \prod_{j=1}^n [\sum_{p=1}^m (l_{ik} * l_{jp} * \Lambda_{ij}(k,p))] \quad (1)$$

Once a formal definition of local consistency such as (1) has been given, it is easy to see that a situation very similar to classical relaxation now holds. However, instead of having to manipulate (1) into a form amenable to iterative solution, we merely note that (1) can be rewritten

$$l_{ik} \leq l_{ik} * \prod_{j=1}^n [\sum_{p=1}^m (l_{jp} * \Lambda_{ij}(k,p))] \quad (2)$$

for every  $i$  and  $k$ . Since the  $l_{ik}$  on the right-hand side is independent of  $j$  and  $p$ . It is clear that if (2) does not hold it can be made to hold by setting  $l_{ik}$  equal to the value on the right-hand side. This is, in fact, equivalent to discarding label  $k$  for  $u_i$  if at some neighbor  $u_j$  there does not exist a compatible label. If the  $l_{ik}$ 's,  $k=1,m$  are now gathered together in vector form:

$$\begin{bmatrix} l_{i1} \\ l_{i2} \\ \vdots \\ l_{im} \end{bmatrix} \leq \begin{bmatrix} l_{i1} \\ l_{i2} \\ \vdots \\ l_{im} \end{bmatrix} * \begin{bmatrix} \sum_{p=1}^m (l_{1p} * \Lambda_{i1}(1,p)) \\ \sum_{p=1}^m (l_{1p} * \Lambda_{i1}(2,p)) \\ \vdots \\ \sum_{p=1}^m (l_{1p} * \Lambda_{i1}(m,p)) \end{bmatrix} * \dots * \begin{bmatrix} \sum_{p=1}^m (l_{np} * \Lambda_{in}(1,p)) \\ \sum_{p=1}^m (l_{np} * \Lambda_{in}(2,p)) \\ \vdots \\ \sum_{p=1}^m (l_{np} * \Lambda_{in}(m,p)) \end{bmatrix} \quad (3)$$

or

$$\begin{bmatrix} l_{i1} \\ l_{i2} \\ \vdots \\ l_{im} \end{bmatrix} \leq \begin{bmatrix} l_{i1} \\ l_{i2} \\ \vdots \\ l_{im} \end{bmatrix} * \begin{bmatrix} L_1 * \Lambda_{i1}(1)' \\ L_1 * \Lambda_{i1}(2)' \\ \vdots \\ L_1 * \Lambda_{i1}(m)' \end{bmatrix} * \dots * \begin{bmatrix} L_n * \Lambda_{in}(1)' \\ L_n * \Lambda_{in}(2)' \\ \vdots \\ L_n * \Lambda_{in}(m)' \end{bmatrix} \quad (4)$$

or

$$L_i \leq L_i * \prod_{j=1}^n \left( \left\{ [L_j] \times [\Lambda_{ij}(1)' \dots \Lambda_{ij}(m)'] \right\}' \right). \quad (5)$$

Let

$$P = \begin{bmatrix} P_1 \\ P_2 \\ P_3 \\ \vdots \\ P_n \end{bmatrix}, \quad (6)$$

where the column vector:

$$P_i = \prod_{j=1}^n (\{[L_j] \times [\Lambda_{ij}(1) \dots \Lambda_{ij}(m)]\}^t). \quad (7)$$

Gathering together the  $L_i$ 's,  $i=1,n$ , we have

$$L \leq L * P \quad (8)$$

This formulation emphasizes the relation to classical relaxation. The relaxation is achieved by repeating

$$L \leftarrow L * P \quad (9)$$

until  $L$  does not change value.

## 2.2 An Example of Region Coloring Problem

Suppose that we are analyzing a picture of a scene, with the aim of describing it, and that we have detected a set of objects  $u_1, \dots, u_n$  in the scene, but have not identified them unambiguously. The relationships that exist among the objects are used to eliminate the ambiguity.

An example for eliminating the ambiguity in a region coloring problem is given here to demonstrate these ideas and computation procedures. For simplicity, consider the case of three regions to be colored red, green or blue with the constraints:

1. Region 1 must be red.
2. Region 3 must be blue, and
3. No two regions may be colored the same color.

Thus,  $u_i = \text{Region } i$  (for  $i=1,2,3$ ) and:

$$U = \{u_1, u_2, u_3\}$$

$$\Lambda = \{\lambda_1, \lambda_2, \lambda_3\}$$

where  $\lambda_1$  is red,  $\lambda_2$  is green, and  $\lambda_3$  is blue. Since region 1 must be red, we have:

$$\Lambda_1 = [1 \ 0 \ 0]^t$$

and since region 3 must be blue:

$$\Lambda_3 = [0 \ 0 \ 1]^t$$

Finally, since there is no restriction on region 2's color, we have all possibilities:

$$\Lambda_2 = [1 \ 1 \ 1]^t$$

Since only similar colors are incompatible, we have:

$$C = \begin{pmatrix} 0 & 1 & 1 \\ 1 & 0 & 1 \\ 1 & 1 & 0 \end{pmatrix} \quad (10)$$

for different objects, and

$$C = \begin{pmatrix} 1 & 0 & 0 \\ 0 & 1 & 0 \\ 0 & 0 & 1 \end{pmatrix} \quad (11)$$

for the same object.

We see then that  $C$  actually depends on the objects under consideration; i.e., technically, we should write  $C_{ij}$  which is identified as:

$$C_{ij} = \begin{pmatrix} Nei(i,j)' & Nei(i,j) & Nei(i,j) \\ Nei(i,j) & Nei(i,j)' & Nei(i,j) \\ Nei(i,j) & Nei(i,j) & Nei(i,j)' \end{pmatrix} \quad (12)$$

where

$$Nei(i,j) = \begin{cases} 0 & \text{if Region } i \text{ does not neighbor Region } j, \\ 1 & \text{if Region } i \text{ does neighbor Region } j. \end{cases}$$

Now we can calculate  $\Lambda_{ij}$  as:

$$\Lambda_{11} = ([1 \ 0 \ 0]^t \times [1 \ 0 \ 0]) * ((0'E) + C) = \begin{pmatrix} 1 & 0 & 0 \\ 0 & 0 & 0 \\ 0 & 0 & 0 \end{pmatrix} * \begin{pmatrix} 1 & 0 & 0 \\ 0 & 1 & 0 \\ 0 & 0 & 1 \end{pmatrix} = \begin{pmatrix} 1 & 0 & 0 \\ 0 & 0 & 0 \\ 0 & 0 & 0 \end{pmatrix} \quad (13)$$

$$\Lambda_{12} = ([1 \ 0 \ 0]^t \times [1 \ 1 \ 1]) * ((1'E) + C) = \begin{pmatrix} 1 & 1 & 1 \\ 0 & 0 & 0 \\ 0 & 0 & 0 \end{pmatrix} * \begin{pmatrix} 0 & 1 & 1 \\ 1 & 0 & 1 \\ 1 & 1 & 0 \end{pmatrix} = \begin{pmatrix} 0 & 1 & 1 \\ 0 & 0 & 0 \\ 0 & 0 & 0 \end{pmatrix} \quad (14)$$

$$\Lambda_{13} = ([1 \ 0 \ 0]^t \times [0 \ 0 \ 1]) * ((1'E) + C) = \begin{pmatrix} 0 & 0 & 1 \\ 0 & 0 & 0 \\ 0 & 0 & 0 \end{pmatrix} * \begin{pmatrix} 0 & 1 & 1 \\ 1 & 0 & 1 \\ 1 & 1 & 0 \end{pmatrix} = \begin{pmatrix} 0 & 0 & 1 \\ 0 & 0 & 0 \\ 0 & 0 & 0 \end{pmatrix} \quad (15)$$

$$\Lambda_{21} = ([1 \ 1 \ 1]^t \times [1 \ 0 \ 0]) * ((1'E) + C) = \begin{pmatrix} 1 & 0 & 0 \\ 1 & 0 & 0 \\ 1 & 0 & 0 \end{pmatrix} * \begin{pmatrix} 0 & 1 & 1 \\ 1 & 0 & 1 \\ 1 & 1 & 0 \end{pmatrix} = \begin{pmatrix} 0 & 0 & 0 \\ 1 & 0 & 0 \\ 1 & 0 & 0 \end{pmatrix} \quad (16)$$

$$\Lambda_{22} = ([1 \ 1 \ 1]^t \times [1 \ 1 \ 1]) * ((0'E) + C) = \begin{pmatrix} 1 & 1 & 1 \\ 1 & 1 & 1 \\ 1 & 1 & 1 \end{pmatrix} * \begin{pmatrix} 1 & 0 & 0 \\ 0 & 1 & 0 \\ 0 & 0 & 1 \end{pmatrix} = \begin{pmatrix} 1 & 0 & 0 \\ 0 & 1 & 0 \\ 0 & 0 & 1 \end{pmatrix} \quad (17)$$

$$\Lambda_{23} = ([1 \ 1 \ 1]^t \times [0 \ 0 \ 1]) * ((1'E) + C) = \begin{pmatrix} 0 & 0 & 1 \\ 0 & 0 & 1 \\ 0 & 0 & 1 \end{pmatrix} * \begin{pmatrix} 0 & 1 & 1 \\ 1 & 0 & 1 \\ 1 & 1 & 0 \end{pmatrix} = \begin{pmatrix} 0 & 0 & 1 \\ 0 & 0 & 1 \\ 0 & 0 & 0 \end{pmatrix} \quad (18)$$

$$\Lambda_{31} = ([0 \ 0 \ 1]^t \times [1 \ 0 \ 0]) * ((1'E) + C) = \begin{pmatrix} 0 & 0 & 0 \\ 0 & 0 & 0 \\ 1 & 0 & 0 \end{pmatrix} * \begin{pmatrix} 0 & 1 & 1 \\ 1 & 0 & 1 \\ 1 & 1 & 0 \end{pmatrix} = \begin{pmatrix} 0 & 0 & 0 \\ 0 & 0 & 0 \\ 1 & 0 & 0 \end{pmatrix} \quad (19)$$

$$\Lambda_{32} = ([0 \ 0 \ 1]^t \times [1 \ 1 \ 1]) * ((1'E) + C) = \begin{pmatrix} 0 & 0 & 0 \\ 0 & 0 & 0 \\ 1 & 1 & 1 \end{pmatrix} * \begin{pmatrix} 0 & 1 & 1 \\ 1 & 0 & 1 \\ 1 & 1 & 0 \end{pmatrix} = \begin{pmatrix} 0 & 0 & 0 \\ 0 & 0 & 0 \\ 1 & 1 & 0 \end{pmatrix} \quad (20)$$

$$\Lambda_{33} = ([0 \ 0 \ 1]^t \times [0 \ 0 \ 1]) * ((0'E) + C) = \begin{pmatrix} 0 & 0 & 0 \\ 0 & 0 & 0 \\ 0 & 0 & 1 \end{pmatrix} * \begin{pmatrix} 1 & 0 & 0 \\ 0 & 1 & 0 \\ 0 & 0 & 1 \end{pmatrix} = \begin{pmatrix} 0 & 0 & 0 \\ 0 & 0 & 0 \\ 0 & 0 & 1 \end{pmatrix} \quad (21)$$

The (p,q) entry of  $\Lambda_{ij}$  tells if  $\lambda_p$  at object i is compatible with  $\lambda_q$  at object j. For example,  $\Lambda_{11}$  reveals that only  $\lambda_1$  is compatible with  $\lambda_1$  at object 1; i.e., that Region 1 must be colored red.

Finally we continue the iteration process. According to Equation (2),

For i=1 and k=1:

$$\begin{aligned} l_{11}^{(n)} \leq & l_{11}^{(n-1)} * [l_{11}^{(n-1)} * \Lambda_{11}(1,1) + l_{12}^{(n-1)} * \Lambda_{11}(1,2) + l_{13}^{(n-1)} * \Lambda_{11}(1,3)] \\ & * [l_{21}^{(n-1)} * \Lambda_{12}(1,1) + l_{22}^{(n-1)} * \Lambda_{12}(1,2) + l_{23}^{(n-1)} * \Lambda_{12}(1,3)] \\ & * [l_{31}^{(n-1)} * \Lambda_{13}(1,1) + l_{32}^{(n-1)} * \Lambda_{13}(1,2) + l_{33}^{(n-1)} * \Lambda_{13}(1,3)] \end{aligned} \quad (22)$$

$$\begin{aligned} 1 \leq & 1 * [1 * 1 + 0 * 0 + 0 * 0] \\ & * [0 * 0 + 0 * 0 + 1 * 1] \\ & * [1 * 0 + 1 * 1 + 1 * 1] \end{aligned}$$

$$1 \leq 1$$

$$1 \leq 1 \text{ which is true}$$

This says that the color red is all right for Region 1. To determine if the color red is possible for Region 2, we must find  $l_{21}$ .

For i=2 and k=1:

$$\begin{aligned} l_{21}^{(n)} \leq & l_{21}^{(n-1)} * [l_{11}^{(n-1)} * \Lambda_{21}(1,1) + l_{12}^{(n-1)} * \Lambda_{21}(1,2) + l_{13}^{(n-1)} * \Lambda_{21}(1,3)] \\ & * [l_{21}^{(n-1)} * \Lambda_{22}(1,1) + l_{22}^{(n-1)} * \Lambda_{22}(1,2) + l_{23}^{(n-1)} * \Lambda_{22}(1,3)] \end{aligned} \quad (23)$$

$$*[l_{31}^{(n-1)}*\Lambda_{23}(1,1)+l_{32}^{(n-1)}*\Lambda_{23}(1,2)+l_{33}^{(n-1)}*\Lambda_{23}(1,3)]$$

$$1 \leq 1*[1*0+0*0+0*0]$$

$$*[1*1+1*0+1*0]$$

$$*[0*0+0*0+1*1]$$

$$1 \leq 1*0$$

$1 \leq 0$  which is false.

Thus,  $l_{21}$  must be set to zero. Likewise, for  $i=2$  and  $k=3$ ,  $l_{23}$  is set to zero, and blue is not a possible label for Region 2. Finally,

For  $i=2$  and  $k=2$ :

$$\begin{aligned} l_{22}^{(n)} \leq & l_{22}^{(n-1)}*[l_{11}^{(n-1)}*\Lambda_{21}(2,1)+l_{12}^{(n-1)}*\Lambda_{21}(2,2)+l_{13}^{(n-1)}*\Lambda_{21}(2,3)] \\ & *[l_{21}^{(n-1)}*\Lambda_{22}(2,1)+l_{22}^{(n-1)}*\Lambda_{22}(2,2)+l_{23}^{(n-1)}*\Lambda_{22}(2,3)] \\ & *[l_{31}^{(n-1)}*\Lambda_{23}(2,1)+l_{32}^{(n-1)}*\Lambda_{23}(2,2)+l_{33}^{(n-1)}*\Lambda_{23}(2,3)] \end{aligned} \quad (24)$$

$$1 \leq 1*[1*1+0*0+0*0]$$

$$*[1*0+1*1+1*0]$$

$$*[0*0+0*0+1*1]$$

$1 \leq 1$  which is true.

We see then that the value of  $l_{11}$ ,  $l_{22}$ , and  $l_{33}$  are not affected by the change of  $l_{21}$  and  $l_{23}$  to zero. In fact, the system of equations stabilizes after the change of  $l_{21}$  and  $l_{23}$ , and the result is  $l_{11} = l_{22} = l_{33} = 1$ , while all other hypotheses are zero. Thus, the only consistent labeling is to label Regions 1,2 and 3 the colors red, green and blue, respectively.

### 3. The Hardware Implementation Problems for DRA

#### 3.1 Assumptions and Statements

To concentrate our attention on tackling the major design complexities without losing generality for developing various DRA architectures, the following assumptions are adopted in our implementations.

Assumption 1: The numbers of objects and labels are assumed to be equal, i. e.,  $n = m$ . Since the extensibility for different numbers of objects and labels has first been considered to be an important factor in system design, DRA2 and DRA3 are able to be specified to an arbitrary number of objects and labels as long as chip size permits [3].

Assumption 2: For useful DRA applications, we have chosen the minimal value of  $n$  and  $m$  to be 8. This is reasonable, for example in image analysis applications.

Assumption 3: Contrary to the assumption in [7] that the input data are always ready before the DRA computation begins, we assume that both data load-in time and their hardware support cannot be ignored in a VLSI DRA computation. This assumption provides a greater challenge for an advanced DRA system implementation.

Assumption 4: The time for binary operation is generally derived from the gate delay of the combinational logic circuits, which is, in our DRA designs, always less than one global clock cycle. Similarly, it is common that one clock cycle is usually less than one Read/Write memory cycle. That is, we have that

$$t_{\text{gate delay}} < t_{\text{clock cycle}} \leq t_{\text{memory R/W cycle}} \quad (25)$$

Whenever we analyze the time complexity, the following three statements hold.

Statement 1: Since the fact that the time complexity for each DRA computing iteration is the same, theoretically, we estimate the time complexity only within one iteration of computation.

Statement 2: As for the worst case of iteration times, which is solely determined by the convergence property of the algorithm and problem feature, we give its estimation in terms of the corresponding VLSI fabrication technology.

Statement 3: We also follow the traditional notation for time complexity analysis for the DRA system, i. e., we describe it according to object number  $n$  and labels number  $m$ , and not the bit number of input data. For example, following statement 1 that, it takes  $O(n)$  time for computing DRA problem in DRA3 architecture, here  $n$  is the number of objects, whereas we have actually loaded in  $n$  by  $m$  bits of input data for each computation.

**3.2 DRA Hardware Implementation Problems**

Definition 4: The DRA2 Hardware Implementation problem has been defined as finding the consistent labeling matrix  $L$ :

$$L=(L_1, L_2, \dots, L_i, \dots, L_n)^t = \begin{pmatrix} l_{11}, l_{12}, \dots, l_{1m} \\ l_{21}, l_{22}, \dots, l_{2m} \\ \dots\dots\dots \\ l_{n1}, l_{n2}, \dots, l_{nm} \end{pmatrix} \tag{26}$$

for the given Region Coloring Problem, provided by the initial labeling matrix:

$$\Lambda=(\Lambda_1, \Lambda_2, \dots, \Lambda_i, \dots, \Lambda_n)^t = \begin{pmatrix} l_{11}^{(o)}, l_{12}^{(o)}, \dots, l_{1m}^{(o)} \\ l_{21}^{(o)}, l_{22}^{(o)}, \dots, l_{2m}^{(o)} \\ \dots\dots\dots \\ l_{n1}^{(o)}, l_{n2}^{(o)}, \dots, l_{nm}^{(o)} \end{pmatrix} \tag{27}$$

and the object-label pairs' compatibility matrices  $C_{ij}$  for every  $i$  and  $j$  ( $i, j = 1, 2, \dots, n$ ).

Definition 5: The DRA3 Hardware Implementation problem has been defined as finding the consistent labeling matrix  $L$ :

$$L=(L_1, L_2, \dots, L_i, \dots, L_n)^t = \begin{pmatrix} l_{11}, l_{12}, \dots, l_{1m} \\ l_{21}, l_{22}, \dots, l_{2m} \\ \dots\dots\dots \\ l_{n1}, l_{n2}, \dots, l_{nm} \end{pmatrix} \tag{28}$$

for the given World Model, provided by the initial labeling matrix:

$$\Lambda=(\Lambda_1, \Lambda_2, \dots, \Lambda_i, \dots, \Lambda_n)^t = \begin{pmatrix} l_{11}^{(o)}, l_{12}^{(o)}, \dots, l_{1m}^{(o)} \\ l_{21}^{(o)}, l_{22}^{(o)}, \dots, l_{2m}^{(o)} \\ \dots\dots\dots \\ l_{n1}^{(o)}, l_{n2}^{(o)}, \dots, l_{nm}^{(o)} \end{pmatrix} \tag{29}$$

and the *object-label pairs' compatibility matrices*  $C_{ij}$  for every  $i$  and  $j$  ( $i, j = 1, 2, \dots, n$ ).

The above definitions represent our research strategy for developing DRA architectures. The DRA2 system is aimed at first reducing both the space and time complexities for a particular DRA application problem, i. e., the region coloring problem. The second one, DRA3 design, generalizes DRA2 for an arbitrary DRA problem and leads to a faster and more general purpose architecture.

#### 4. A Conventional DRA1 Design and the Complexity Analysis

The entire DRA computation consists of mainly two parts. The first part generates the  $n^2$   $m$  by  $m$  compatibility matrices for object pairs  $u_i$  and  $u_j$ ; i. e., computing each matrix  $\Lambda_{ij}(k,p)$  ( $i, j = 1, \dots, n$ ;  $k, p = 1, \dots, m$ ) from the most recently evaluated (or originally given at the first iteration) labelings; as depicted in Eq.s (13) to (21). The second part as shown in Eq.s (22) to (24), is an iteration process for the relaxation of the current object pairs' constraints among all different objects to produce new labelings; i. e., computing each new labeling  $l_{ik}$  ( $i = 1, \dots, n$ ;  $k = 1, \dots, m$ ), provided by the currently known object constraint matrices  $\Lambda_{ij}(k,p)$ . Reviewing the DRA formulation and the computational procedure for the region coloring example in section 2 reveals the complexity issues met in the DRA1 system design.

Time Complexity: With Eq.s (22) - (24), at least  $n \times m$  memory Read/Write operations must be performed for computing an  $n$  by  $m$  matrix of  $l_{jp}^{(n-1)} \times \Lambda_{ij}(k,p)$  elements. Because there are  $n \times m$  iteration equations (for computing new labels  $l_{ik}$ , where  $i = 1, \dots, n$ ;  $k = 1, \dots, m$ ) which need to be evaluated, the sequential computation time would be  $O(n^2 m^2)$ . In the first DRA1 design, in addition to using the sequential evaluation strategy, another  $O(m)$  time is spent on the complicated nested control loop for memory Read/Write operations during each iteration evaluation [11,13]. Thus the entire computation time within each iteration costs  $O(n^2 m^3)$ . There are other binary computations which must be taken into account. According to assumption 4, their contributions compared to R/W operations of memory are ignored.

Space Complexity: During each iteration of DRA computation, several intermediate arguments (initial arguments at the first iteration) take certain amounts of space be stored. The initial label matrix  $\Lambda$  ( $L^{(0)}$  matrix) and the next iteration result of  $\Lambda$  each takes  $O(n^2)$  space. The matrices  $\Lambda_i \times \Lambda_j^{-1}$  and the label pairs compatibility matrices  $C_{ij}(k,p)$  as well as the resulting object pairs compatibility matrices  $\Lambda_{ij}(k,p)$  ( $i, j = 1, \dots, n$ ;  $k, p = 1, \dots, m$ ) each takes  $O(n^2 m^2)$  space. The total space complexity is:

$$O(2n^2 + 3n^2m^2) = O(n^2m^2). \quad (30)$$

**Data Routing Complexity:** It is meaningful to consider the routing complexity only if a parallel DRA architecture may possibly exist. We are to discuss this issue in section 5 and section 6 when developing parallel DRA architectures. In fact, the data routing complexity during each iteration is over  $O(n^2m^2)$ . For an 8-object 8-label DRA parallel system, there are at least 8K data being routed or communicated during each iteration.

The DRA1 architecture, unfortunately, serially computes each intermediate element. The computation strategy imbedded in this design is purely *I/O-bound*. Assuming  $t_{\text{read}} \approx t_{\text{write}} \approx 500$  ns for an NMOS process and the time complexity is  $O(n^2m^3)$  of each iteration. Multiplying the possible maximum iteration times, which is on the order of  $O(nm)$  and is determined by the feature of the computational model [9], the worst case execution time is over seconds or minutes. For practical applications, the number of objects could be 8, 16 or 32, the corresponding memory requirements for these different cases are 8K, 32K and 128K, respectively. As shown in the DRA1 design, this has greatly added to the circuit size which has been a bottleneck in DRA1 system design when  $n$  becomes larger.

## 5. Parallel Tree-root Pipelining and the DRA2 System

In the analyses above, most of the computing time was spent on the R/W operations for matrices  $\Lambda_{ij}(k,p)$ ; moreover, one half of the  $O(n^2m^2)$  space is taken for the generation of matrices  $\Lambda_{ij}(k,p)$ , which blocks the DRA1 VLSI computation. In this section we describe a DRA2 architecture which is completely independent of the  $\Lambda_{ij}(k,p)$  evaluation [11].

### 5.1 A Parallel Tree-Structured Reformulation for DRA

It should be clear that any attempt to speed up an *I/O-bound* computation must rely on an increase in the memory bandwidth [39]. Speeding up a compute-bound computation, however, may frequently come from the concurrent use of many processing elements [39-44]. The degree of parallelism in a special-purpose system is largely determined by the underlying algorithm. In order to solve the complexity arising in the conventional DRA1 design, the following three steps have been taken to design a hardware algorithm that supports a high degree of concurrency in DRA computation.

#### 1. Constructing the Parallel Computation Tree

When more effort is spent analyzing Eq. (2), we see that element  $\Lambda_{ij}(k,p)$  can be decomposed as:

$$\Lambda_{ij}^{(n-1)}(k,p) = l_{ik}^{(o)} l_{jp}^{(o)} C_{ij}(k,p) \tag{31}$$

which can form a leaf node like:

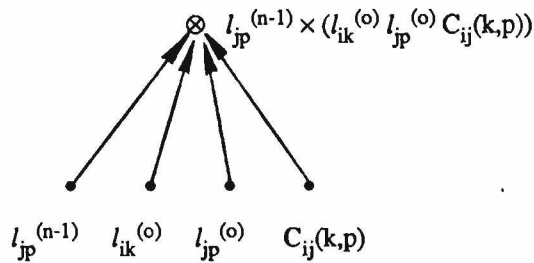


**Figure 1:** Leaf Node for Computing  $l_{jp} \times \Lambda_{ij}(k,p)$

so that Eq. (2) can be hierarchically formed as a tree-like structure with each level imbedded in the parallel computation for their leaves' operands as shown in Figure 3.

### 2. Speeding Up Iteration

Once a DRA problem in processing is identified as convergent, its current computing labeling reaches its final consistent labeling asymptotically in such a way that the error vectors, i. e., the difference vectors between these two labelings, monotonically decrease. Therefore, the node computation in Figure 1 can be speeded up by replacing the initial given elements  $l_{ik}^{(o)}$  and  $l_{jp}^{(o)}$  with the most recently  $n-1$ <sup>th</sup> iterated results  $l_{ik}^{(n-1)}$  and  $l_{jp}^{(n-1)}$ . The modified computation composed of the leaf node:

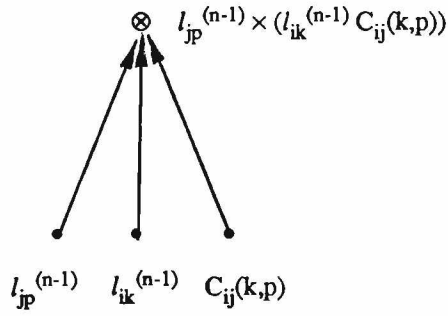


Figure 2: Modified Leaf Node Computation for  $l_{jp} \times \Lambda_{ij}(k,p)$

The computation tree for  $l_{ik}^{(n)}$  is formed as:

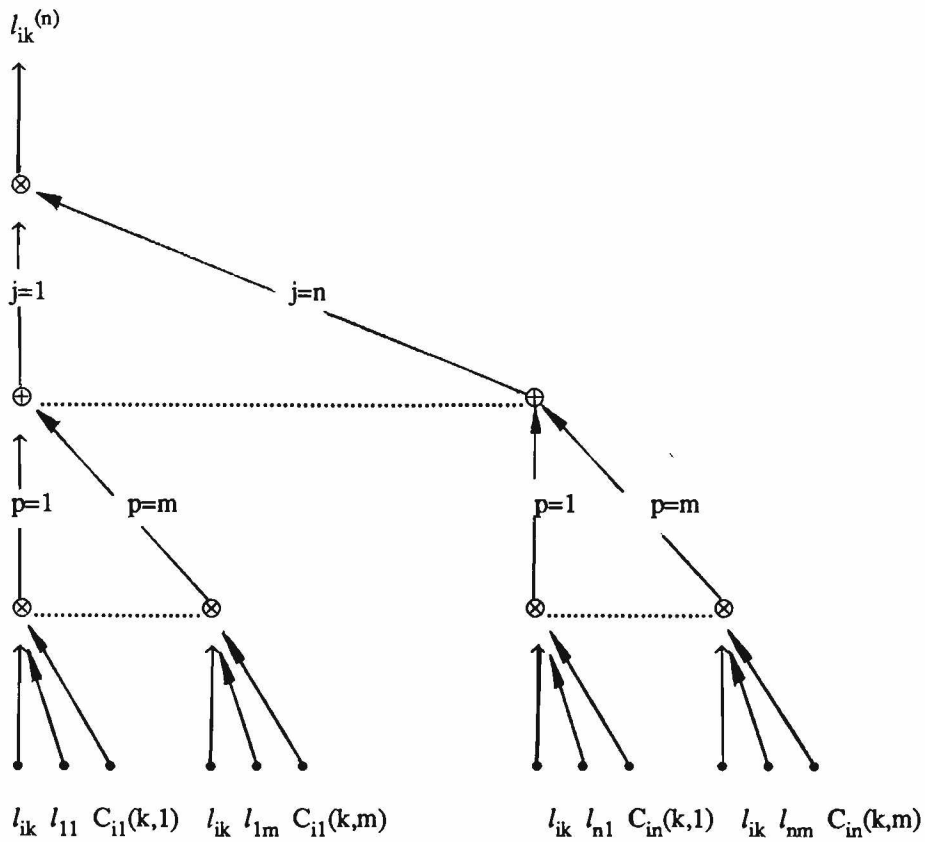


Figure 3: A Parallel Tree for Computing  $n^{th} l_{ik}$

In section 5.2 it is shown that the bottommost leaves' operands have been associated with a data pipelining channel, completing a multiple parallel tree-root pipelining scheme which supports a highly concurrent DRA computation. For convenient notation in the rest of the paper, we classify these three kinds of bottommost leaves' operands of Figure 3 in:

**Definition 6:** (1) We define the labeling elements of the  $l_{jp}$ 's ( $j = 1, \dots, n$  and  $p = 1, \dots, m$ ), which are inside the pipelining channel, to be *l-pipe*; and those on the tree root to be *l-root*. Both *l-pipe* and *l-root* have the same logic values except they are topologically separated in the system layout. (2) Signal  $l_{ik}$  passes through all roots horizontally through each row array of  $k$ ; it is defined as the broadcasting signal  $b_k$ . (3) The  $C_{ij}(k,p)$  matrix elements, which are systematically distributed along each tree root, are defined as the  $C_{ij}(k,p)$ -Pattern.

### 3. Introducing a Time Dimension in the Computation

To compute an  $n$ -object  $m$ -label DRA problem, a total of  $n$  by  $m$   $l_{ik}$ 's need to be evaluated. This means at least 64 computation trees as shown in Figure 3 need to be built inside the circuit for our  $n = m = 8$  case, which greatly increases the circuit size. To minimize this problem, each operand at the bottom of the tree has been constructed in a time-dimension. As the time changes forward, different  $l_{ik}$ 's ( $i = 1, \dots, n$ ;  $k = 1, \dots, m$ ) can be generated. These time-varying characteristics can best be described by the following *spatial-temporal (ST) index equations*:

$$i \leftarrow i+t \bmod n, \quad (32)$$

$$j \leftarrow j+t \bmod n. \quad (33)$$

denoted by  $A \leftarrow B$  or we say that  $A$  is generated by  $B$ . We call  $i$ , or  $i+t$ , and  $j$ , or  $j+t$  the spatial-temporal indexes since they characterize the indexes in the recursive formulas of Eq.s (1-9). They constitute the theoretical basis for the recursive systolic computation and interleaved processing in the DRA2 and DRA3 systems, while the basic DRA-PE cell realizes the computation in the formula. It is also of interest to see that in the DRA2 system [11], the ST indexes generates the dynamic forward DRA computational wavefront on a statically configured DRA architecture; while in the DRA3 architecture [12], it forms the dynamically configurable DRA3 architectural wavefront for a virtually static computation.

## 5.2 Implementation Issues for the DRA2 Chip

### 1. System Architecture and Block Diagram

The block diagram of the DRA2 circuit is illustrated in Figure 4. The chip consists of four functional blocks.

1. **Compatibility Matrix Registers (CMR).  $C_{ij}$  Registers** are a set of eight 8-bit shift registers in the leftmost part of the circuit; they are used for storing each  $C_{ij}$  matrix. Another set of  $C_{ij}$  Registers in the rightmost part of the circuit are for storing  $C_{ij}$ .
2.  **$8 \times 8$  Multiprocessor SIMD Array (MSA).** The MSA is composed of 8 by 8 simple and regular cells. They are predefined to map the highly parallel computation algorithm of Figure 3 onto silicon. A number of parallel horizontal and vertical communication wires are designed around the four edges of the cells to make use of higher degrees of parallelism in the computation.
3. **L-matrix Shift Register (LSR).** It is used for (1) the input and output data paths for the original and final labeling matrices, (2) the pipelining channel for tree-root operand broadcasting and pipelining, forming a recursive DRA computational wavefront, and (3) performing temporarily the data storing and updating.
4. **Control Module (CM).** This module includes four units. An **8-Bit Comparator** is located on top of the first 8-bit shift register of the LSR to sense the equality between the  $n^{\text{th}}$  output vector  $L_i^{(n)}$  of the MSA array and the corresponding  $n-1^{\text{th}}$  row vector  $L_i^{(n-1)}$  inside the LSR. A **Timer** is served as both the systole pacer and tagged-bit signal generator for iteration control. An **8-Bit State Register** is used for collecting comparison results from the Comparator and monitoring iteration states. Finally a **Finite State Machine (FSM)** is built for performing a self-timed synchronization among these functional blocks and host computer.

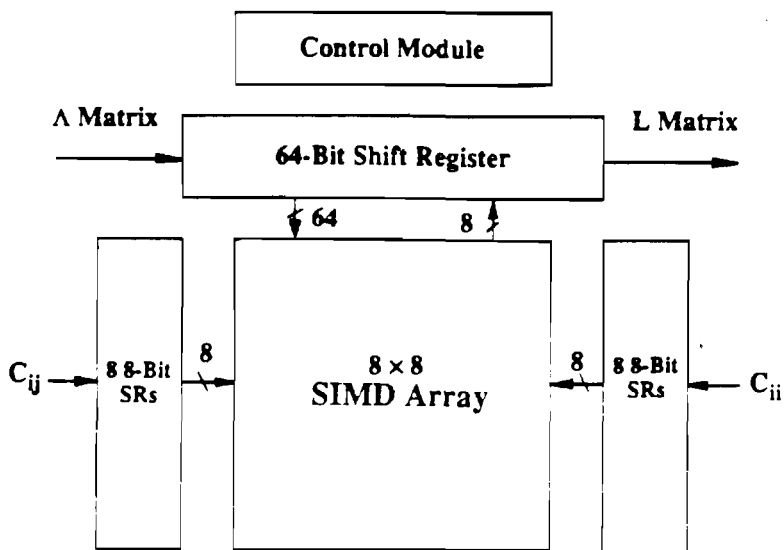


Figure 4: Circuit Block Diagram for the DRA2 System

This diagram of four functional blocks also serves as the PPL layout floor plan for efficient layout (in subsection 5.4).

## 2. Multiprocessor SIMD Array and the Cell Design

The basic principle of the Multiprocessor SIMD architecture for DRA2 is illustrated in Figure 5. By replacing a single Processing Element with an array of 8 by 8 PEs, a higher computation throughput can be achieved without increasing memory bandwidth. The function of the memory (i.e., the L matrix shift registers) in the diagram is to pulse data  $l\text{-pipe}_{jp}$  ( $j = 1, \dots, n; p = 1, \dots, m$ ) through the array of cells. Then new data  $l\text{-pipe}_{ik}$  ( $i = 1, \dots, n; k = 1, \dots, m$ ) are returned to memory in a rhythmic fashion. The crux of this approach is to ensure that once the data are brought out from the memory they can be used effectively at each cell they pass while being pumped through the entire array.

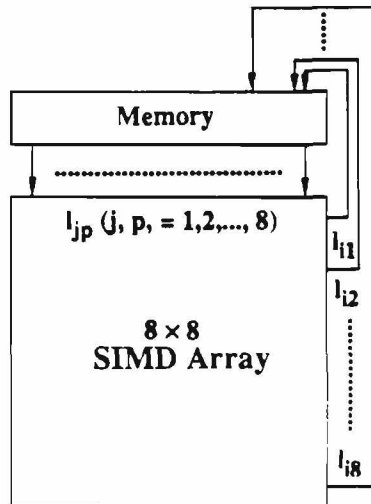
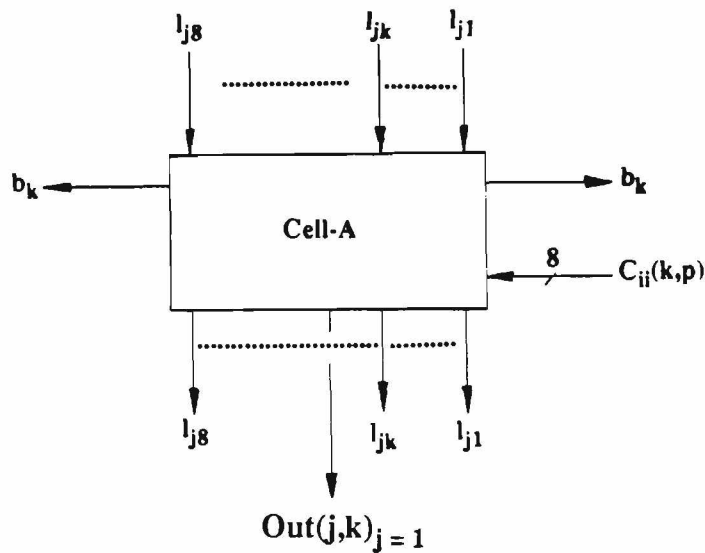


Figure 5: Basic Principle of the Parallel DRA2 System

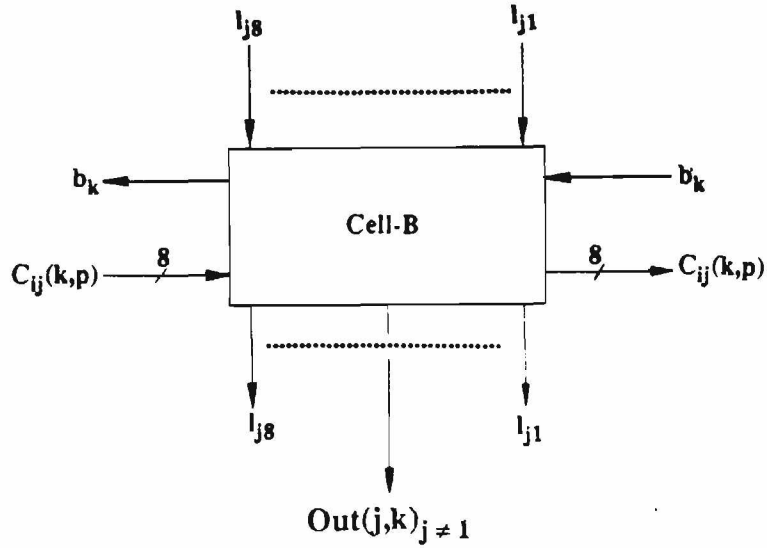
To perform the parallel DRA2 computation, two cells (as illustrated in Figure 6 (a) and (b)) with almost identical logic and structure were used in constructing the entire array. The only difference is that the first cell performs the generation of the multiple broadcasting signals  $b_k$  ( $k = 1, \dots, m$ ) for each row array while the second cell is only transparent to the passing of the  $b_k$  signals. The construction of the multiprocessor SIMD array using these two cells is illustrated in Figure 7.



$$b_k = l_{jk}, \text{ at column } j_1.$$

$$Out(j,k)_{j=1} = \sum_{p=1}^m (l_{jp} \times \Lambda_{ij}(k,p)) = \sum_{p=1}^m (l_{jp} \times l_{ik} \times C_{ii}(k,p)) = \sum_{p=1}^m (l_{jp} \times b_k \times C_{ii}(k,p)) = \sum_{p=1}^m (\overline{l_{jp} + b_k + C_{ii}(k,p)}). \quad (35)$$

(a) Cell-A



$$b_{k(in)} = b_{k(out)}, \text{ at columns } j \neq 1. \quad (36)$$

$$Out(j,k)_{j \neq 1} = \sum_{p=1}^m (l_{jp} \times \Lambda_{ij}(k,p)) = \sum_{p=1}^m (l_{jp} \times l_{ik} \times C_{ij}(k,p)) = \sum_{p=1}^m (l_{jp} \times b_k \times C_{ij}(k,p)) = \sum_{p=1}^m (\overline{l_{jp} + b_k + C_{ij}(k,p)}). \quad (37)$$

(b) Cell-B

Figure 6: Two Cells in Multiprocessor DRA2 Array

According to Figure 3 and equations (34) to (37), these two cells are implemented in two levels of NOR gate combinational logic. Their PPL [36] layouts can be easily identified in Figure 13.

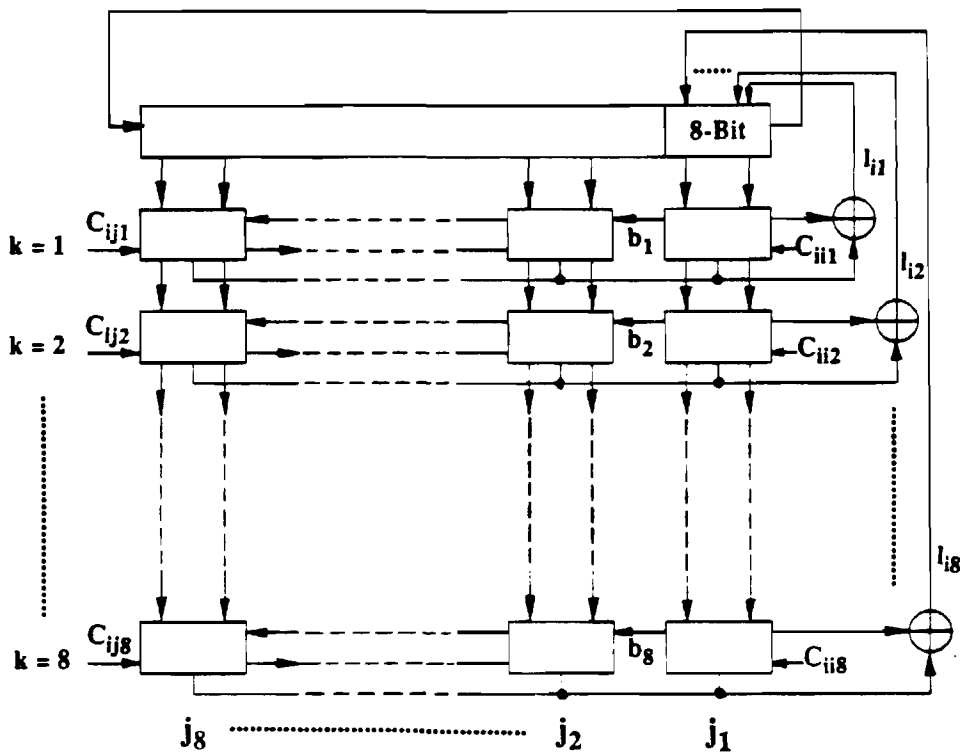


Figure 7: Construction of SIMD Multiprocessor Array Using Cell-A and Cell-B

We see from Figure 6 that in essence the inner summation part of Equation 2 is carried out in Cell-A and Cell-B, while the outer multiplication part of that equation is implemented in each horizontal array in Figure 7.

It is also noted from Figure 6 and 7 that the DRA2 architecture can readily be extended to different numbers of objects and labels. For example, a row array of the number  $k$  in Figure 7 can be added in order to attach one more label for all objects, while a column array of the number  $j$  in the same Figure can be added to extend the system for one more object, provided that the corresponding changes inside each cell are made. The critical analysis indicates that the DRA2 systems for 8, 16, and 32 objects are technically implementable in the 3.0  $\mu$  NMOS, 2.0  $\mu$  and 1.2 CMOS, and 1.0  $\mu$  GaAs processes [14].

### 3. Circuit Features and Design Techniques

In addition to designing the simple and regular cells, several efficient techniques, such as interleaved processing, multiple signal broadcasting, and self-timed synchronization, were applied to the implementation of the SIMD multiprocessor DRA2 architecture.

Recursive Systolic Computation and Interleaved Processing

Since the introduction of the time dimension in subsection 5.1, the multiprocessor SIMD array in Figure 7 possesses a time-varying characteristic which makes recursive systolic computation and interleaved processing possible. Let's focus on the first column ( $j = 1$ ) array. It is clearly indicated that the first input vector, which is the  $i^{\text{th}}$  row vector of  $L$ , the labeling matrix, at the  $n-1^{\text{th}}$  iteration, is fed into the first column of DRA2 array as

$$(l_{j1}, l_{j2}, l_{j3}, \dots, l_{jm}),$$

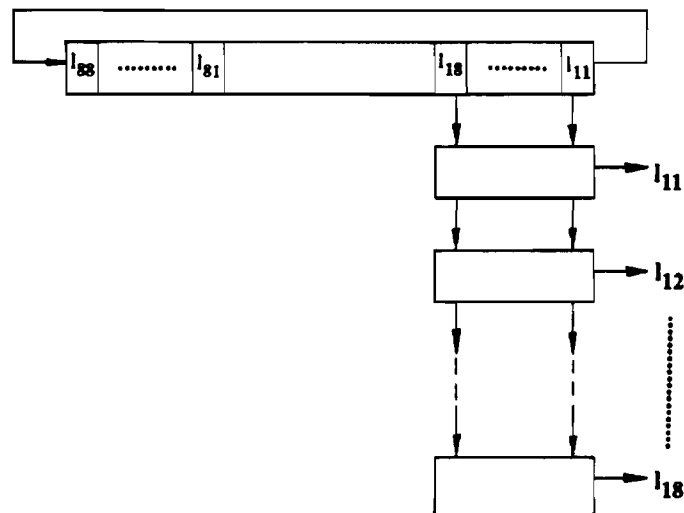
where  $j = 1, \dots, n$ . The corresponding output vector  $L_i$  of the multiprocessor SIMD array, which is the  $i^{\text{th}}$  row vector of  $L$  labeling matrix at the  $n^{\text{th}}$  iteration, is generated:

$$(l_{i1}, l_{i2}, l_{i3}, \dots, l_{im}),$$

where  $i$  is fixed at a time  $t = i$ . As time moves forward, the elements in the  $L$  shift register have shifted from the left to the right in an 8-clock-pulse fashion. For example, in the DRA2 system, at time  $t = i = 1$ , vector  $L_1$

$$(l_{11}, l_{12}, l_{13}, l_{14}, l_{15}, l_{16}, l_{17}, l_{18})$$

is generated.



and at time  $t = i = 2$ , vector  $L_2$

$$(l_{21}, l_{22}, l_{23}, l_{24}, l_{25}, l_{26}, l_{27}, l_{28})$$

is generated, etc.

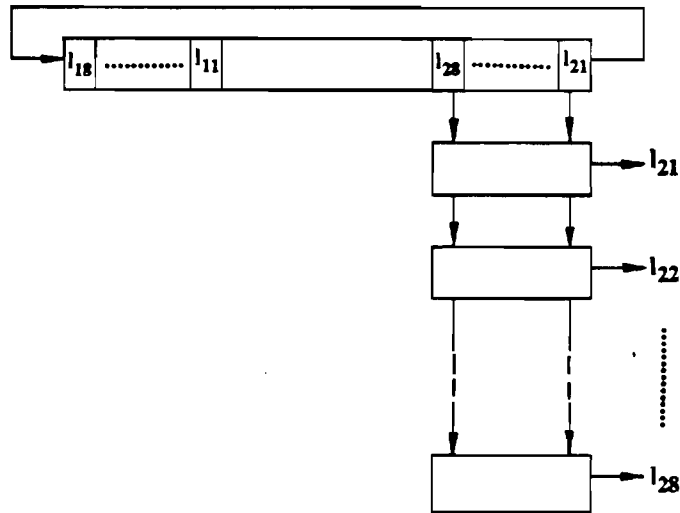


Figure 8: Computational Wavefront Pipelining and Circulation for Interleaved Processing

Each  $L_i$  vector is computed based on the interleaved utilization of the multiprocessor SIMD array, whereas eight  $L_i$  vectors form an entire computational wavefront of the  $L$  labeling matrix, of the  $n^{\text{th}}$  relaxation iteration. Note that we use  $n$  computing trees for generating  $n \times m$   $l_{ik}$ 's in  $O(nm)$  time; we may also use  $O(nm)$  computing trees to compute the same number of  $l_{ik}$ 's in  $O(n)$  time, provided that the latter has a uniformly progressing wavefront in time and in space.

Multiple Signal Broadcasting

The broadcasting technique is probably one of the most obvious ways to make multiple use of each input element. It plays an important role in making the parallel computation tree of Figure 3 implementable. Two multiple broadcasting schemes are used in DRA2 architecture. In the first,  $n$  by  $m$  vertical broadcasting lines from each pipelining operand are connected to the bottom most leaves' node of each parallel computing tree (passing each  $l$ -pipe to  $l$ -root). Secondly, as depicted in Figures 6 and 9, Cell-A at column  $j (=1)$  is used to jog signal  $l_{ik}^{(n-1)}$  (which is the  $n^{\text{th}}$   $l$ -pipe $_{jp}$ ) and then propagate it horizontally from right to left through the entire row array. Thus, the output vector of the multiprocessor SIMD array, i.e.,  $(l_{i1}, l_{i2}, l_{i3}, l_{i4}, l_{i5}, l_{i6}, l_{i7}, l_{i8})$ , can be generated simultaneously in a highly concurrent manner.

Definition 7: The second multiple data routing scheme for jogging  $b_k$  at column  $j = 1$ , as illustrated in Eq.s (32) and (34), and Figure 9, is defined as the *J-Pattern*.

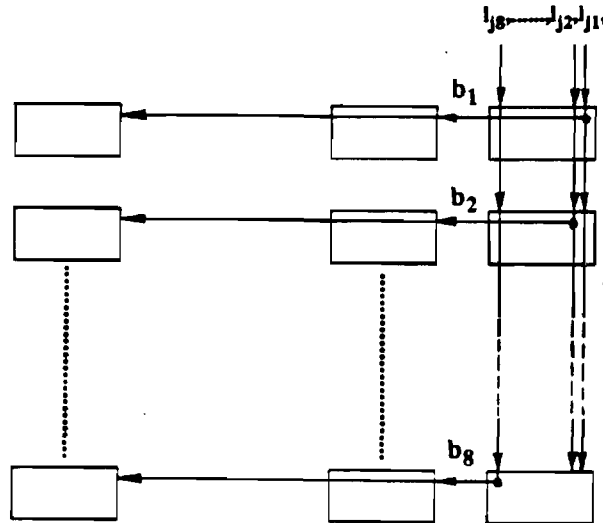
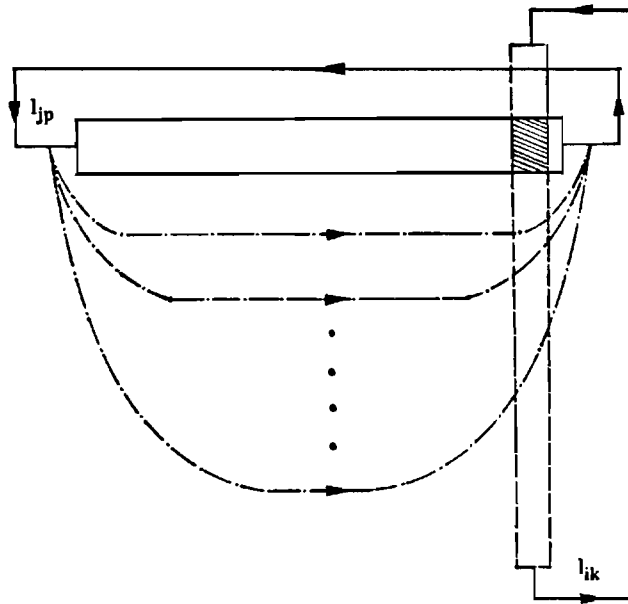


Figure 9: Broadcasting Scheme for the  $b_k$  Signals

Cross Circle Associative Pipelining

Much associativity is introduced through the associative circular pipelining in the DRA2 design. Refer Figures 7, 8, 9 and 10, two circular pipelining loops are implemented.

The first pipelining is designed for  $l_{jp}$  elements. This pipelining can be viewed in two parts, master pipelining part and slaver pipelining part. The master pipelining refers a serial horizontal circular pipelining of the  $l_{jp}$  elements inside the main pipelining channel, LSR. While the master pipelining is going on, a parallel horizontal virtual circular pipelining is followed in  $k$  row horizontal arraies. The parallel pipelining in DRA array is a slaver pipelining of the master one which is supported by multiple signal broadcasting.



**Figure 10:** Associative Circular Pipelining

Viewing the Figure 10, the second pipelining for  $l_{ik}$  is a parallel vertical circular pipelining which is crossed the serial horizontal pipelining at the rightmost first  $m$ -bit of the main pipelining channel, to update the old labels in the channel with new labels.

In addition to providing impressive parallelism, an extra advantage of these pipelining schemes is that it decreases the routing and control complexities.

#### Self-Timed Synchronization and Tagged-Bit Control

By using recursive systolic computation and interleaved processing, the computational task has been decomposed into the smallest computing piece,  $L_i$ . To compute each vector  $L_i$ , the globally synchronized multiprocessor SIMD array of Figure 7 is used. For completing the entire relaxation computation, this synchronous array is imbedded into a self-timed system. The self-timed asynchronous scheme may be costly in terms of extra hardware and delay in each element, but it has the advantage that the time required for a communication event between two elements is independent of the size of the entire system [44]. Also, it is easy to design and validate a self-timed state machine in PPL methodology [37].

Among the 64-bit L shift registers, the rightmost first 8-bit SR is one which is able to parallel load in the  $n^{\text{th}}$  output

vector from the multiprocessor SIMD array in order to update the current  $n-1^{th}$   $L_i$  row vector. This iteration and updating process is the core of the relaxation process described in Eq. (8). To sense the completion of computation, a Comparator is built on top of the first 8-bit SR. If two vectors are equal, a **row-eq** signal of 1 is produced and stored into **8-bit States SR** of the Control Module; otherwise a 0 signal is sent. As soon as the State Register gets eight 1's, which means the equality of Eq. (8) is reached, an **all-eq** signal is issued to the FSM. Since the control processes in this system are based on the data validity of a *control data flow*, reliable and fast execution in a data-driven environment is created. The control mechanism used in the parallel DRA2 architecture is shown in Figure 11.

To ensure that the iteration cycle completes at the end of  $n \times m$  cycles, a **tagged-bit** is derived from an ANDed term of both the  $l_{11}$  bit and the 64th-count of the Timer, which has served as a reliable alignment signal for computation in the control flow.

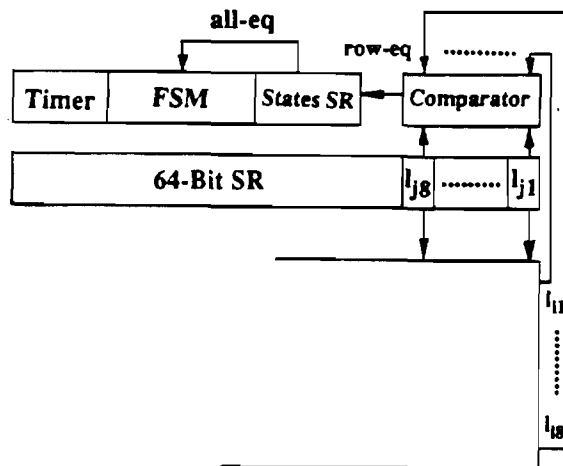


Figure 11: Self-Timed Synchronization

In Figure 12 the state graph of the FSM is illustrated.

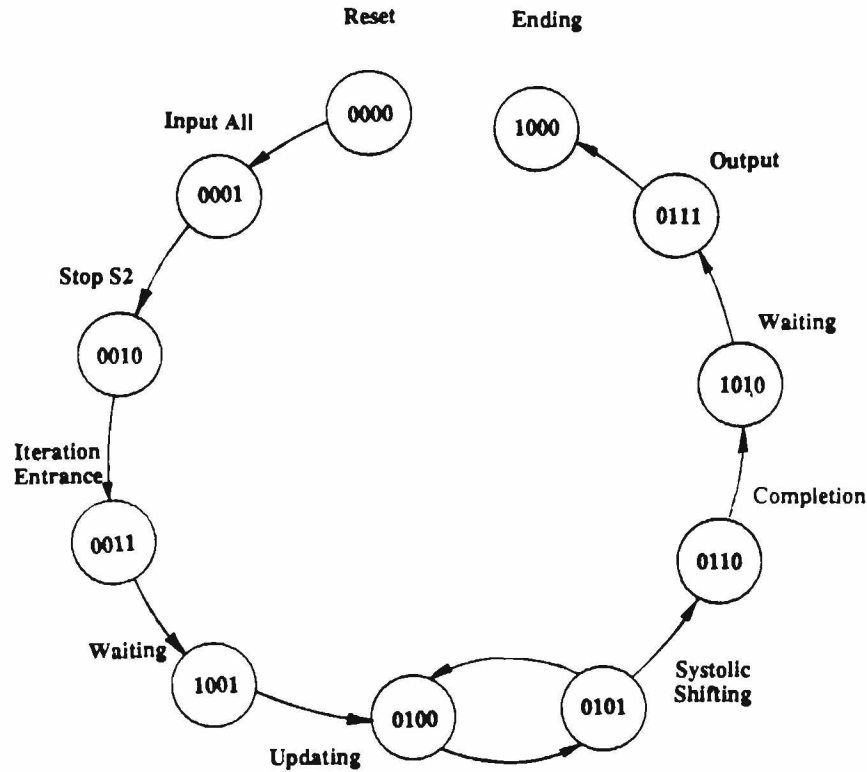


Figure 12: State Graph of the Finite State Machine

### 5.3 Performance Evaluation

With the parallel tree-structured reformulation and tree-root pipelining in its system design, the DRA2 architecture takes advantage of a high degree of pipelining and multiprocessing. It gets rid of the need for storing and computing each element associated with the object pairs matrices  $\Lambda_{ij}(k,p)$ . One-half of the  $O(n^2m^2)$  space is eliminated; the other half is reserved for input data  $C_{ij}(k,p)$ , the label pairs compatibility matrices. In certain DRA computations, as shown in the *Region Coloring Problem*, the space complexity can even be reduced to  $O(nm)$ ; i. e., only an  $O(nm)$ -bit shift register is required to store all  $n$  by  $m$  intermediate (or original) labeling elements [11]. Obviously, the DRA2 computation during each iteration only takes  $O(nm)$  clock cycles. Assuming a clock cycle is about 120ns (using a  $3\mu$  NMOS process and the PPL design methodology), DRA2 performs the DRA computation in microseconds, and in the worst case, i.e., multiplying the maximum possible iteration time,  $O(nm)$ , in milliseconds [11,15].

#### 5.4 The PPL Layout for DRA2 System

The DRA2 chip was built by assembling the four functional blocks in Figure 4 using PPL (Path Programmable Logic) tools at the University of Utah [36]. Since parallel computation and the multiprocessor SIMD array greatly simplify the design difficulties, the PPL layout is very simple and straightforward. An overview of the complete PPL layout, which is a PPL mapping of the block **floor plan** in Figure 4, is shown in Figure 13.

For details associated with the complete system design, the simulation results, interfacing strategy with host computer, timing and wiring delay analysis, testing, pinout description, and fabrication of the DRA2 chip see [11,15].



**Figure 13:** The PPL Layout of the Multiprocessor SIMD DRA2 System

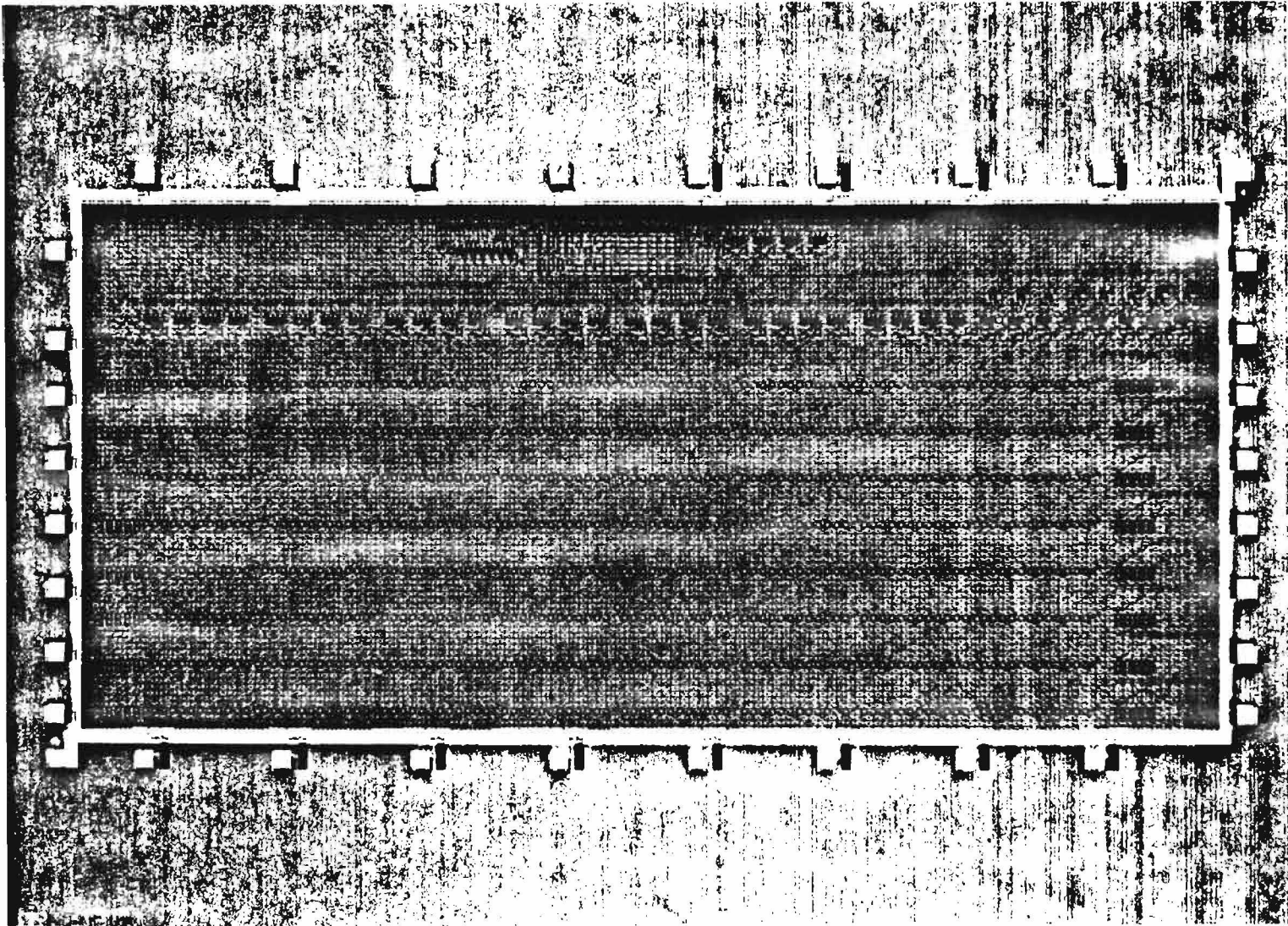


Figure 14: The Photomicrograph of the DRA2 Chip

## 6. An $O(n)$ Time Algorithm-Configured Dynamic Architectural Wavefront System

Compared to the conventional DRA1 design, the DRA2 system achieves a very impressive performance improvement in terms of speed, size, and memory access requirements. However, there are still several bottlenecks in developing a fast general purpose DRA architecture.

### 6.1 Complexity Issues Revisited

Time Complexity: The  $O(nm)$  time of the DRA2 system is suitable only for a small number of objects, though the number of objects and labels in DRA2 architecture can be extended to a larger number of objects and labels. The larger the number of objects and labels are, the slower the DRA2 system becomes. It is desirable that a much faster DRA architecture be designed for real-time processing of a larger number of objects and labels.

Data Preprocessing Complexity: One of the remarkable characteristics of the DRA problem is that a large number of data, such as  $O(n^2m^2)$  elements of label pairs compatibility matrices  $C_{ij}(k,p)$ , must be loaded into the system before the computation is performed. In addition to this, the data ordering and format which might be processed during the load-in time must be arranged to support efficient DRA computation. Following assumption 3, the term *Data Preprocessing Complexity (DPC)* is used here to refer to the complexity issues which arise in the analysis of the time and space, as well as hardware complexities in this kind of data-preprocessing-intensive VLSI computation. Some labeling solutions avoid this problem by assuming that the data is always ready for computation.

Data Routing Complexity: One of the proposed DRA3 architectures [12] is shown in Figure 18, in which the data routing complexity in the horizontal direction between two DRA modules is of  $O(m^2)$ ; a total of  $O(nm^3)$  connections are required for  $nm$  DRA modules to be routed. The data routing complexity becomes another dominant factor in designing the DRA3 system as the number of labels increases.

Fabrication Difficulty: Although we have separated the main pipelining channel and have used the larger buffers to drive between shift registers, its characteristic turns out to be worse as the numbers of  $n$  and  $m$  increase.

### 6.2 $C_{ij}(k,p)$ -Pattern Distribution Analysis

The DRA3 architecture overcomes these difficulties based on the use of the dynamically configured architectural wavefront on the DRA3 switch lattice [12]. It runs the DRA computation in  $O(n)$  time without the extra

requirement for data preprocessing hardware and without requiring the horizontal routing among the DRA modules, provided that only an  $O(nm^2)$  number of switches must be added to the original multiple broadcasting wires of the DRA2 system.

In fact, computing time, data preprocessing complexity, and data routing complexity form a coherent mixture in the DRA3 system design. We illustrate its major architectural concepts beginning with the analysis of  $C_{ij}(k,p)$ -Patterns in the case of  $n = m = 3$ .

Referring to Eq. (2) and Figure 8, the first computational wavefront for computing the  $n^{\text{th}}$  labels  $l_{ik}^{(n)}$  is formed at time  $t = i = 1$  as:

For  $i = 1$  and  $k = 1,2,3$ :

$$l_{1k}^{(n)} \leq l_{1k}^{(n-1)} * [l_{11}^{(n-1)} * \Lambda_{11}(k,1) + l_{12}^{(n-1)} * \Lambda_{11}(k,2) + l_{13}^{(n-1)} * \Lambda_{11}(k,3)] \\ * [l_{21}^{(n-1)} * \Lambda_{12}(k,1) + l_{22}^{(n-1)} * \Lambda_{12}(k,2) + l_{23}^{(n-1)} * \Lambda_{12}(k,3)] \\ * [l_{31}^{(n-1)} * \Lambda_{13}(k,1) + l_{32}^{(n-1)} * \Lambda_{13}(k,2) + l_{33}^{(n-1)} * \Lambda_{13}(k,3)].$$

A snapshot of the  $C_{ij}(k,p)$  ( $j, k, p = 1,2,3$ ) matrix data distribution pattern which is matched with the  $l_{1k}^{(n)}$  wavefront at  $t = 1$  is:

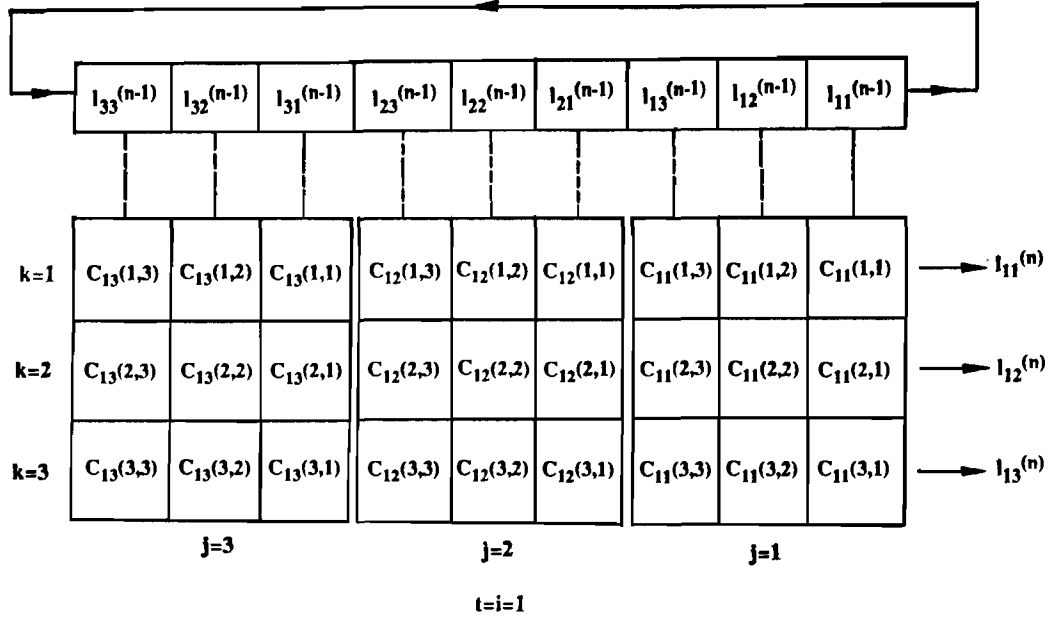


Figure 15: The  $C_{1j}(k,p)$  Pattern for generating  $l_{1k}$ 's

At time  $t = 2$ , a computational wavefront for generating  $l_{2k}^{(n)}$  is produced. For  $i = 2$  and  $k = 1, 2, 3$ :

$$\begin{aligned}
 l_{2k}^{(n)} \leq & l_{2k}^{(n-1)} * [l_{11}^{(n-1)} * \Lambda_{21}(k,1) + l_{12}^{(n-1)} * \Lambda_{21}(k,2) + l_{13}^{(n-1)} * \Lambda_{21}(k,3)] \\
 & * [l_{21}^{(n-1)} * \Lambda_{22}(k,1) + l_{22}^{(n-1)} * \Lambda_{22}(k,2) + l_{23}^{(n-1)} * \Lambda_{22}(k,3)] \\
 & * [l_{31}^{(n-1)} * \Lambda_{23}(k,1) + l_{32}^{(n-1)} * \Lambda_{23}(k,2) + l_{33}^{(n-1)} * \Lambda_{23}(k,3)].
 \end{aligned}
 \tag{39}$$

The  $C_{2j}(k,p)$  ( $j, k, p = 1, 2, 3$ ) matrices distribution pattern at this time is:

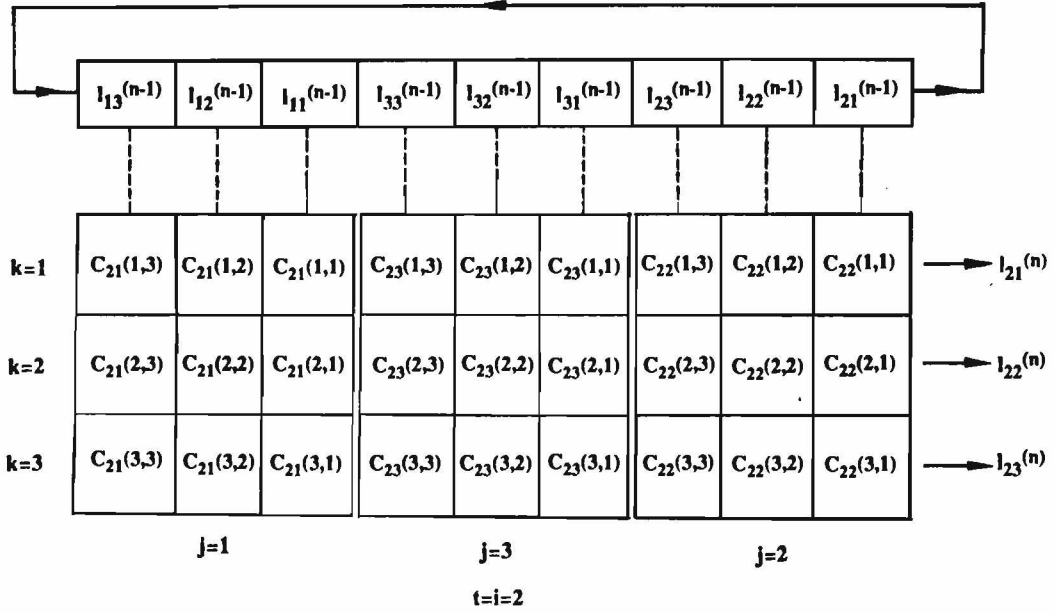


Figure 16: The  $C_{2j}(k,p)$  Pattern for generating  $l_{2k}$ 's

From Figures 15 and 16, several criteria for DRA3 architecture are derived.

(1) At time  $t = i$ , to compute each new labeling vector  $L_i$ , different computational wavefronts are formed and the associated  $C_{ij}(k,p)$  matrices are distributed. More accurately, at time  $t$ , each matrix  $C_{ij}(k,p)$  elements (where  $t, j = 1, \dots, n$  and  $k, p = 1, \dots, m$ ) stored in the  $k^{th}$  row of a parallel memory in Figures 14 and 15 are retrieved. Thus a parallel Row-Readable RAM is required.

(2) It is clearly indicated that the  $C_{ij}(k,p)$  elements associated with each dynamically pipelined operand in the main tree-root pipelining channel are one unit of  $j$  skewed and horizontally circulated. The cyclic shifting of the bits of  $C_{ij}(k,p)$ -Patterns elements to the right for  $m$ -bit position corresponds to a *Block-data Shuffling* operation [43]. We summarize and extend all distributed C matrices' patterns in Figure 17. (Each symbol actually is a matrix distributed in Figures 15 and 16.)

$t = 1:$	$C_{13}(k,p)$	$C_{12}(k,p)$	$C_{11}(k,p)$
$t = 2:$	$C_{21}(k,p)$	$C_{23}(k,p)$	$C_{22}(k,p)$
$t = 3:$	$C_{32}(k,p)$	$C_{31}(k,p)$	$C_{33}(k,p)$

**Figure 17:** A Circularly Skewed  $C_{ij}(k,p)$ -Pattern when Generating  $l_{ik}$ 's

The first requirement requires a simple associative processing, i.e., parallel Row-Readable RAMs; while the second criterion demands higher order design complexity in time and data preprocessing, as well as in data routing.

A candidate design for the DRA3 system, where  $n = m = 8$ , is presented in Figure 18. The DRA3 system is made up of using 8 by 8 DRA modules. Each module consists of a PE cell (same structure as Cell-A and Cell-B in DRA2 system) and a local Row-Readable parallel RAM for  $C_{ij}(k,p)$ -Pattern.

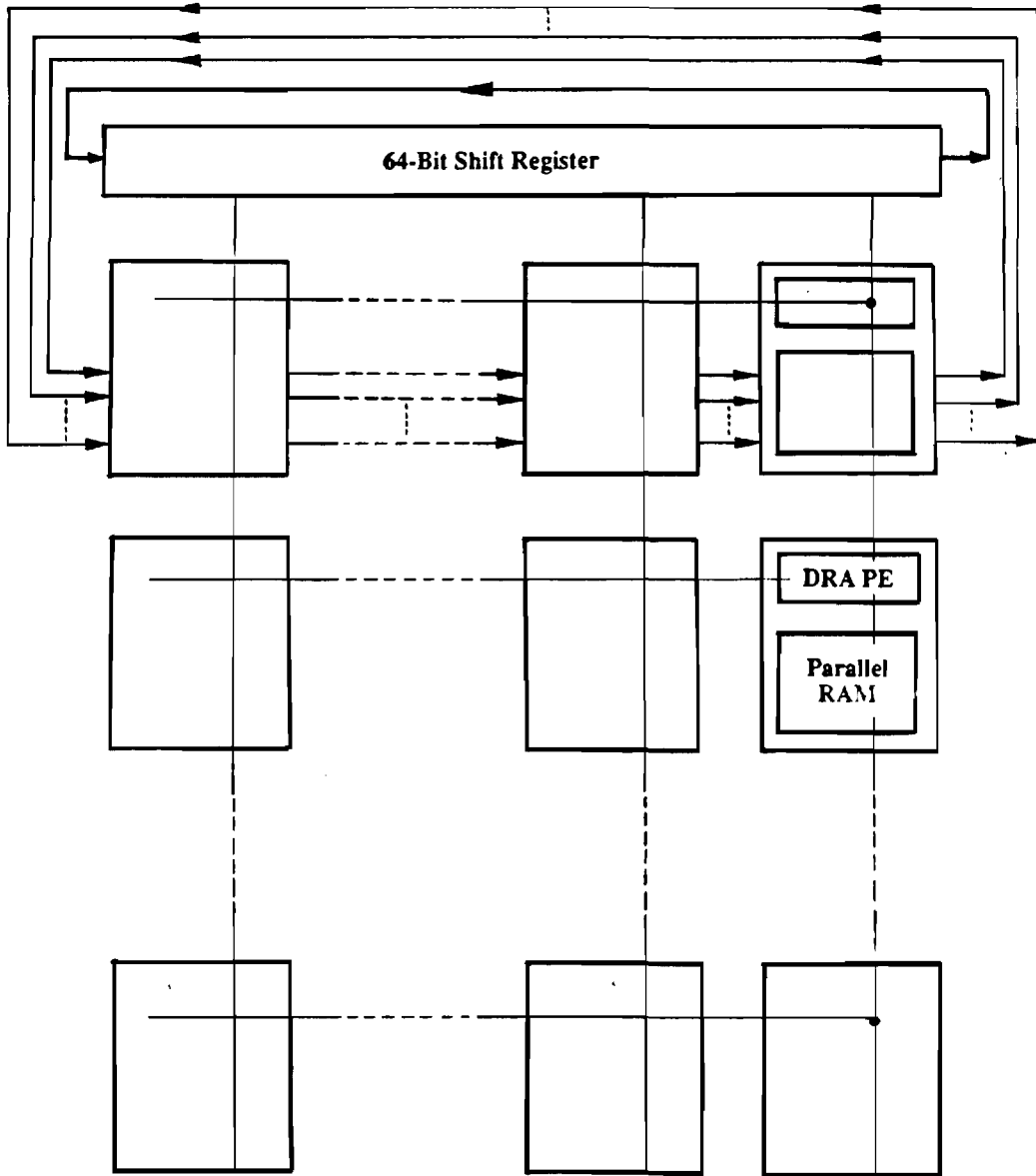


Figure 18: A Candidate Design for DRA3 System

A pre-shuffling chip is implemented and fabricated using a 3  $\mu$  NMOS PPL design methodology in order to make the  $C_{ij}(k,p)$ -Pattern the same format as in Figure 17 [16]. However the pre-processing hardware costs  $O(b^3)$  time (noting that  $b$  is the number of bits to be shuffled) and takes more than half of the chip, provided that a difficult inter-chip routing problem remains unsolved [12].

### 6.3 A Dynamically Configurable DRA3 Architecture

The configurable, highly parallel computer system is a multiprocessor architecture that provides a programmable interconnection structure integrated with the PEs [10]. The original idea is that, the computer processing begins with the controller broadcasting a command to all switches to invoke a particular *static* configuration setting. The design of the DRA3 system has revealed that by adopting an advanced *dynamic* configuring strategy on the DRA3 switch lattice, not only can the DRA computational wavefront be generated while retaining the benefits of uniformity and locality that DRA-PE exploits, but also the combined limitations imposed in upgrading DRA3 architecture can be completely eliminated.

#### 1. The Architectural-Computational Wavefront (ACW) Notation

We rewrite Weiser and Davis's definition of wavefront [38]:

**Definition 8:** A *wavefront*, denoted as  $A$ , represents an ordered set of data elements:  $\{a(1,m), a(2,m), \dots, a(N-1,m), a(N,m)\}$ , where  $m$  is the "time" subscript. The elements  $a(i,m)$  for all  $m$  belong to the  $I^{\text{th}}$  data stream. For simplicity, the "time" subscript in the elements of a wavefront is omitted and  $a(i,m)$  will be simply be represented as  $a(i)$ .

We extend the definition as:

**Definition 9:** The *Architectural-Computational Wavefront (ACW) Notation* [12] consists of two different wavefronts. The *Computational Wavefront* is an ordered set of data elements:  $\{c(1,i+t), c(2,i+t), \dots, c(N,i+t)\}$ , where  $i+t$  is the spatial-temporal index in Eq. (32). The *Architectural Wavefront* is an ordered set of architectural configurations:  $\{a(1,j+t), a(2,j+t), \dots, a(N,j+t)\}$ , where  $j+t$  is the spatial-temporal index in Eq. (33).

The following distinctions are made which are necessary for building a DRA3 system:

1. The computational wavefront dynamically progresses on a static architecture, as the *ST* indexes increase. The architectural wavefront progresses, by dynamically configuring the system architecture, in a way against the computational wavefront, as the *ST* indexes increase. For instance, as we have seen that the *ST* index in DRA2 forms a dynamic DRA computational wavefront on a static DRA2 architecture; we will show see that the *ST* index of DRA3 generates a dynamic DRA3 architectural wavefront for a virtual static DRA computation.
2. The equivalence between computational wavefront and architectural wavefront holds. Thus either one characterizes both of them.
3. Both architectural and computational wavefront notation have spatial parameters, such as *i* and *j*, and temporal parameter, such as *t*, so that both can be manipulated on the space and time domains.
4. The conventional wavefront notation assumes a uniform progression of the data stream. This restriction is eliminated by combining *ST* indexes with ACW notation, as is obvious that these indexes may behave synchronously or asynchronously.
5. The ACW notation first differentiates the computational wavefront and architectural wavefront and is more suitable for exploring architectural configurability and the synthesis of highly configurable system.

Referring to Eq.s (2), (32), and (33), there is always a data dependence relation among these arguments with respect to time *t* and positions *k* and *j*, that:

$$l\text{-pipe}_{i+t,k}^{(n)} \leftarrow \sum_{p=l}^m l\text{-root}_{i+t,k}^{(n-1)} l\text{-root}_{j+t,p}^{(n-1)} C_{i+t,j+t}(k,p). \quad (40)$$

In Figure 7 we see that this data dependency equation is topologically mapped onto silicon in terms of the parallel tree structure. The vertical broadcasting of the *l-pipe* operands from pipelined channel to DRA array is described by a routing function:

$$l\text{-pipe}_{i+t,k}^{(n-1)} \rightarrow l\text{-root}_{j+t,p}^{(n-1)} \downarrow C_{i+t,j+t}(k,p), \quad (41)$$

where the symbol  $\downarrow$  denotes an alignment relation such that  $A \downarrow B$  if and only if *A* and *B* have the same physical column position of *j*. The J-Pattern of definition 7 is routed by equation:

$$l-root_{j+t,p}^{(n-1)} \rightarrow l-root_{i+t,k}^{(n-1)} \updownarrow C_{i+t,j+t}(k,p). \quad (42)$$

The DRA computation is valid if and only if these two dependency equations are true at any time  $t$  and positions  $k$  and  $j$ , as well as the iteration times  $n$ . Eq. (41) stands for a static network in the DRA3 architecture. Eq. (42) is a virtually static network; a potential speed-up in the DRA3 computation can be reached by dynamic configuring Eq. (41) in an ACW notation.

## 2. Dynamic Configuring the DRA3 Architectural Wavefront

Though symbol  $j$  represents the horizontal spatial shifting (in Figures 15 and 16) while the symbol  $t$  represents the temporal unit, the computational wavefront progression of  $l-root_{j+t,p}$  proceeds (referring to Eq.s (32) and (33)) as the increasing of  $j+t$ , where the combined parameter  $j+t$  must not be associated with any dimensions. By definition 9, it is obviously correct that the  $l_{ik}$  computational wavefront moves from left to right, as the  $ST$  indexes increase and is equivalent to that of the J-Pattern (one configuration of the architectural wavefront) shifts in the reverse horizontal direction, as the  $ST$  indexes increase. The DRA computation can be performed by manipulating *either* a computational wavefront *or* configuring dynamically an architectural wavefront.

In Figure 19, we create a dynamically configurable DRA3 architectural wavefront by building an algorithm-configured switch lattice. A total number of  $O(nm^2 + nm)$  switches are added between each vertical wire and horizontal wire.

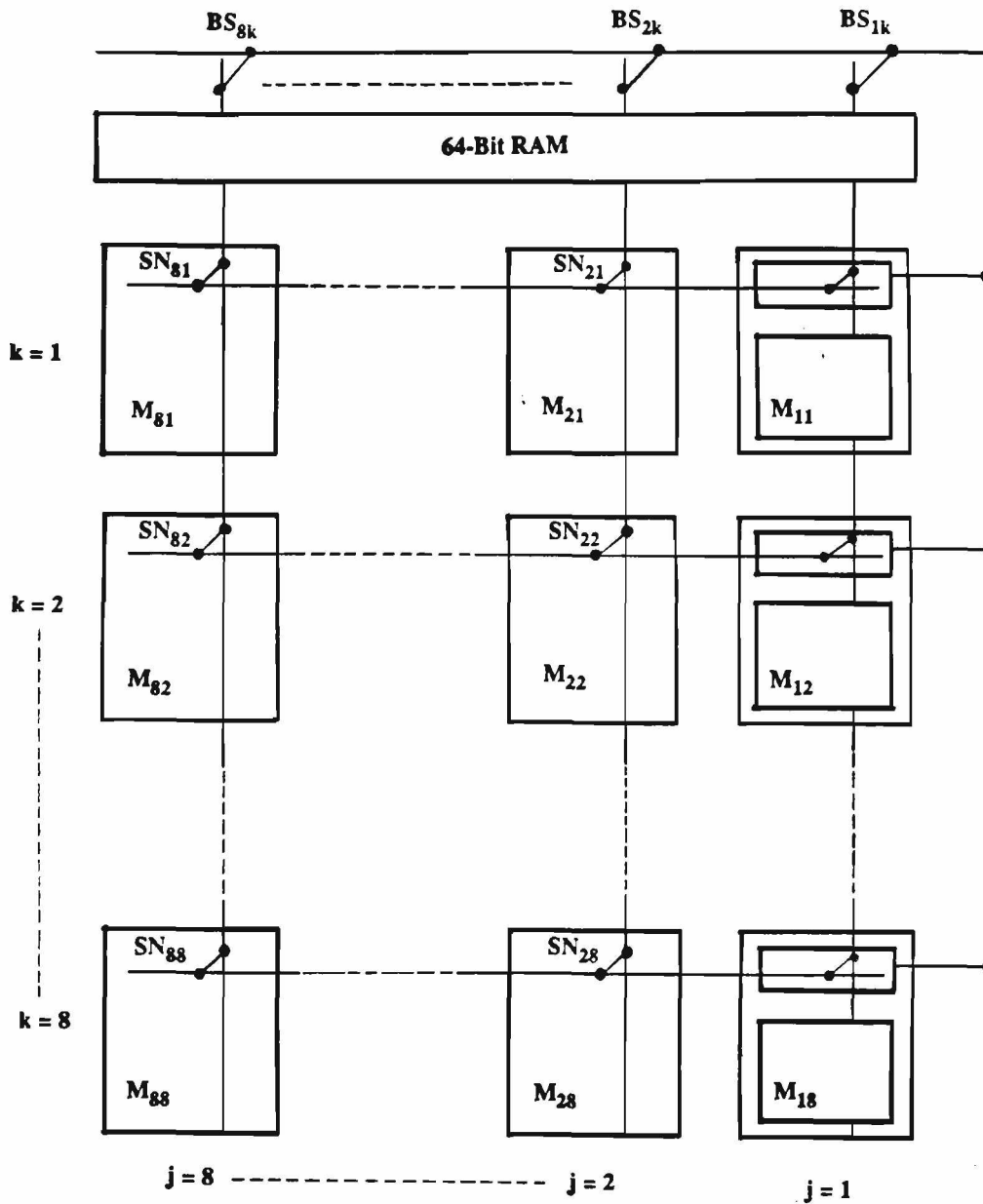


Figure 19: The DRA3 Architecture

In Figure 19, there are  $n$  by  $m$  identical DRA modules denoted by  $M_{jk}$  ( $j = 1, \dots, n$  and  $k = 1, \dots, m$ ). Let  $SN_{jk}$  denote a Switching Node which connects vertical broadcasting wire  $l_{jk}$  and horizontal broadcasting wire  $b_k$  inside of each Module. Let  $BS_{jk}$  denote a Bus Switch which connects the labeling output of the multiprocessor SIMD array to the

operands of the "pipelining channel," noting that the pipelining channel is now static and is replaced with an  $O(nm)$ -bit RAM. These switches are programmed by a *Self-Timed System Controller*, as is shown in DRA2 circuit, to avoid the time delay occurred during the broadcasting on the switch lattice. For DRA3 computation, we give:

**Definition 10:** We define the *DRA3 architectural wavefront* to be the interconnection patterns of the DRA3 switch lattice, of which both the switches  $SN_{jk}$  for a column  $j$ , i.e., the J-Pattern at a specified column  $j$ , and switches  $BS_{jk}$  for that column  $j$  are invoked simultaneously, where index  $j$  is defined in Eq. (33).

During the DRA3 computation, at index  $j \pmod n$ , the DRA3 architectural wavefront shifts from right to left in  $O(n)$  clock cycles, therefore, an entire DRA computation, which is virtually static, is dynamically generated.

It would now be of interest to examine whether the complexity issues in section 6.1 are solved upon building the DRA3 architecture. First, a time upper bound of  $O(n)$  is reached. Secondly, there is no particular hardware support and no special requirements for data-preprocessing. Under dynamic parallel configuring of DRA3, the  $C_{ij}(k,p)$ -Pattern is naturally distributed in matrix index order in the original parallel memory. For an intuitive understanding, we redraw the  $C_{ij}(k,p)$ -Pattern of Figure 17 in Figure 20 which is associated with DRA3 computation strategy.

$$\begin{array}{rcll}
 t = 1: & C_{13}(k,p) & C_{12}(k,p) & C_{11}(k,p) \\
 t = 2: & C_{23}(k,p) & C_{22}(k,p) & C_{21}(k,p) \\
 t = 3: & C_{33}(k,p) & C_{32}(k,p) & C_{31}(k,p)
 \end{array}$$

**Figure 20:** A  $C_{ij}(k,p)$ -Pattern under Dynamic Reconfiguration of DRA3

The third problem, an intensive multiple data routing requirement is eliminated by adding  $O(nm^2 + nm)$  switches on the DRA3 switch lattice. As for the long pipelining channel, it is replaced with  $O(nm)$  bits of smaller and more reliable RAM cells, under the dynamic data routing. Finally, since  $C_{ij}(k,p)$ -Pattern is designed for  $O(n^2)$  arbitrary  $m$  by  $m$  C-matrices, the DRA3 system is good for any general purpose DRA computation.

## 7. Conclusions

We have described several VLSI architectures for speeding up the computation of the Discrete Relaxation

Algorithm. The key issues are a new tree-root pipelining scheme and a technique to dynamically configure the architectural wavefront. The implementations of these architectures offer much greater processing performance than general purpose processors. Further research in this area is to imbed the highest degree of flexibility in DRA design by allowing programmability in cells as well as reconfigurability of cell interconnections, for generating efficient and faster dynamically configurable MIMD DRA architectures.

## REFERENCES

1. D. H. Ballard and C. M. Brown, *Computer Vision*, Prentice-Hall, Inc., Englewood Cliffs, New Jersey, 1982.
2. B. K. P. Horn, *Robot Vision*, The MIT Press, Cambridge, 1986.
3. J. Ullman, *An Algorithm for Subgraph Homomorphisms*, In *J. ACM*, Vol. 23, pp. 31-42, Jan. 1976.
4. R. M. Haralick and L. G. Shapiro, *The Consistent Labeling Problem: Part 1*, In *IEEE Trans. on Pattern Analysis and Machine Intelligence*, Vol. PAMI-1, No. 2, pp. 173-184, April, 1979.
5. R. M. Haralick and L. G. Shapiro, *The Consistent Labeling Problem: Part 2*, In *IEEE Trans. on Pattern Analysis and Machine Intelligence*, Vol. PAMI-2, No. 3, pp. 193-203, May, 1980.
6. B. Nudel, *Consistent-Labeling Problems and their Algorithms: Expected-Complexities and Theory-Based Heuristics*, In *Artificial Intelligence*, Vol. 21, pp. 135-178, 1983.
7. J. T. Mccall, J. T. Tront, F. G. Gray, R. M. Haralick and W. M. McCormack, *Parallel Computer Architectures and Problem Solving Strategies for the Consistent Labeling Problem*, In *IEEE Trans. on Computer*, Vol C-34, No. 11, pp. 973-980, November 1985.
8. R. Mohr and T. C. Henderson, *Arc and Path Consistency Revisited*, In *Artificial Intelligence*, Vol. 28, pp. 225-233, 1986.
9. T. C. Henderson, *Discrete Relaxation*, Oxford University Press, London, to appear.
10. L. Snyder, *Introduction to the Configurable, Highly Parallel Computer*, In *IEEE Computer*, pp. 47-56, January, 1982.
11. W. Wang, J. Gu and T. C. Henderson, *A Pipelined Architecture for Parallel Image Relaxation Operations* In *IEEE Trans. on Circuits and Systems*, Vol. CAS-34, No. 11, 1987. A detailed version is in *Technical Report, UUCS-TR-86-008*, Department of Computer Science, University of Utah, March, 1987.
12. J. Gu, W. Wang and T. C. Henderson, *An  $O(n)$  Time Discrete Relaxation Architecture for Real-Time Processing of the Consistent Labeling Problem*, *Technical Report, UUCS-TR-86-116*, Department of Computer Science, University of Utah, December, 1986.
13. D. Ku, *DRA1 Chip Implementation Report*, Project Report, Department of Computer Science,

- University of Utah, March, 1986.
14. M. Gaspar, *Discussion with the PPL Design Methodology and MOSIS Fabrication Technology*, Private Communication, December, 1986.
  15. MOSIS, *DRA2 Chip Fabrication Report*, Information Science Institute, University of Southern California, December, 1986.
  16. W. Burger, *A Virtual Shuffle Dynamic RAM Controller*, Project Report, Department of Computer Science, University of Utah, February, 1986.
  17. A. Ginzberg, *Algebraic Theory of Automata*, Academic, New York, 1968.
  18. F. Harary, *Graph Theory*, Addison-Wesley, Reading, 1969.
  19. R. V. Southwell, *Relaxation Methods in Engineering Science*, Oxford University Press, London, 1940.
  20. D. Waltz, *Understanding Line Drawings of Scenes with Shadows*, In P. H. Winston (editor), *Psychology of Computer Vision*, pp. 19-91, McGraw-Hill, New York, 1975.
  21. A. Rosenfeld, R. A. Hummel and S. W. Zucker, *Scene Labeling by Relaxation Operations*, In IEEE Trans. on Systems, Man, and Cybernetics, Vol. SMC-6, No. 6, pp. 420-433, June 1976.
  22. J. P. A. Deutsch, *A Short Cut for Certain Combinational Problems*, In Proceedings of the British Joint Comput. Conference, 1966.
  23. R. E. Fikes, *REF-ARF: A System for Solving Problems Stated as Procedures*, In Artificial Intelligence, Vol. 1, pp. 27-120, 1970.
  24. A. Bundy (editor), *Catalogue of Artificial Intelligence Tools*, In *SYMBOLIC COMPUTATION Artificial Intelligence*, L. Bolc, A Bundy, P. Hayes and J. Siekmann (editors), Springer-Verlag, Berlin, 1984.
  25. E. C. Freuder, *Synthesizing Constraint Expressions*, In Comm. ACM, Vol. 21, No. 11, 1978.
  26. R. Kowalski, *A Proof Procedure Using Connection Graphs*, In J. ACM, Vol. pp. 572-595, October, 1975.
  27. R. M. Haralick and J. Kartus, *Arrangements, Homomorphisms, and Discrete Relaxation*, In IEEE Trans. on Systems, Man, and Cybernetics, Vol. SMC-8, No. 8, pp. 600-612, August, 1978.
  28. E. G. Whitehead, Jr., *Combinatorial Algorithm*, Courant Inst. Mathematical Sciences, New York University, 1972.

29. C. Eastman, *Preliminary Report on A System for General Space Planning*, In Comm. ACM, Vol. 15, pp. 76-87, 1972.
30. R. W. Grossman, *Some Data Base Applications of Constraint Expressions*, Research Technical Report, LCS-158, MIT, 1976.
31. A. Newell and H. A. Simon, *Human Problem Solving*, Prentice-Hall Inc., Englewood Cliffs, 1972.
32. A. Nijenhuis and H. S. Wilf, *Combinatorial Algorithms*, Academic Press, New York, 1975.
33. U. Montanari, *Networks of Constraints: Fundamental Properties and Applications to Picture Processing*, In Inform. Sci., Vol. 7, pp. 95-132, 1974.
34. A. Rosenfeld, *Networks of Automata: Some Applications*, In IEEE Trans. on Systems, Man, and Cybernetics, Vol. SMC-5, pp. 380-383, 1975.
35. D. L. Waltz, *Generating Semantic Descriptions from Drawings of Scenes with Shadows*, MIT Technical Report A1271, November, 1972.
36. K. F. Smith, T. M. Carter and C. E. Hunt, *Structured Logic Design of Integrated Circuits Using the Storage/Logic Array (SLA)*, In IEEE Trans. on Electron Devices, Vol. ED-29, No. 4, April, 1982.
37. A. B. Hayes, *Self-Timed IC Design with PPL's*, In R. E. Bryant (editor), *Proceedings of the Third CalTech Conference on VLSI*, pp. 257-273, Computer Science Press, Rockville, January, 1983.
38. U. Weiser and A. Davis, *A Wavefront Notation Tool for VLSI Array Design*, In H. T. Kung, B. Sproull and G. Steele (editors), Proceedings of CMU Conference on VLSI System and Computations, pp. 226-234, Computer Science Press, October 1981.
39. H. T. Kung, *Putting Inner Loops Automatically in Silicon*, Lecture Notes in Computer Science Vol. 163: VLSI Engineering, pp. 70-104, Edited by Tosiyasu L. Kunii, Springer-Verlag, 1985.
40. J. Miklosko and V. E. Kotov, *Algorithms, Software and Hardware of Parallel Computers*, Springer-Verlag, Berlin, 1984.
41. S. Y. Kung, et al., *Wavefront Array Processor: Language, Architecture, and Applications*, In IEEE Trans. on Computer, Vol. C-31, No. 11, pp. 1054-1066, November 1982.
42. D. J. Kuck, *The Structure of Computers and Computations Vol. 1*, John Wiley & Sons, New York, 1978.
43. K. Hwang and F. A. Briggs, *Computer Architecture and Parallel Processing*, McGraw-Hill, New

York, 1984.

44. C. Mead and L. Conway, *Introduction to VLSI Systems*, Addison-Wesley Publishing Company, Reading, 1980.